



Research Paper

Study of the mineralogical and textural properties of bricks with volcanic ash temper

María López Gómez^{*}, Giuseppe Cultrone

Department of Mineralogy and Petrology, Faculty of Sciences, University of Granada, Avda. Fuentenueva, s/n, 18002 Granada, Spain

ARTICLE INFO

Keywords:

La Palma (Canary Islands)
Fired bricks
Reuse of volcanic ash
Mineralogical changes

ABSTRACT

During the eruption of the Tajogaite volcano in La Palma (Canary Islands, Spain) in 2021, large amounts of pyroclastic material were emitted, which had severe environmental, health and economic impacts on nearby localities. One solution for the disposal of the volcanic ash that settled on the streets, roads, and roofs of La Palma is to use it as temper in brick production, which would also reduce the amount of clay required to make the bricks. Two different sizes (fine and coarse) and three percentages (10, 20, and 30 % by weight) of volcanic ash were added to a clayey sediment from Viznar (Granada, Spain) to produce bricks that were fired at 800, 950, and 1100 °C in an electric oven with an oxidising atmosphere. The chemistry, mineralogy and texture of the samples with volcanic ash were compared to control samples made without it and fired at the same temperature. In the bricks with ash there was a reduction in the phases detected in the control samples (quartz, phyllosilicates, and newly formed gehlenite, and diopside) and augite, a phase present in the volcanic ash, appeared. The volcanic ash fragments in the samples fired at over 950 °C turned red in color, owing to the formation of iron oxides. The increase in the concentration of volcanic ash caused a progressive increase in the vitreous phase and in clinopyroxene. Conversely, there were no significant differences in terms of their mineralogical composition between the fired bricks made with fine or coarse ash, although the samples with coarse volcanic ash apparently showed higher porosity.

1. Introduction

Large amounts of lava and pyroclastic materials are generated during a volcanic eruption. These materials can have negative effects on public health and the economy in the surrounding areas, as well as on the global environment. Lava fluxes do not usually cause human casualties due to the low velocity at which they advance, although they have severe economic impacts as they destroy everything in their path, such as buildings, roads, and crops (Kilburn, 2015).

Pyroclastic materials is a generic term used to describe the particles emitted during a volcanic eruption. They can be subdivided according to their size into bombs (>64 mm), lapilli (64–2 mm), and ash (<2 mm) (Fisher and Schmincke, 1984). When these materials reach populated areas, they can damage buildings and infrastructure for example, by corroding metalwork, reducing traction and visibility on the roads and obstructing filters, and the deposit of large amounts of volcanic ash on the roofs of buildings can lead to their collapse (Wilson et al., 2015). Volcanic ash can also affect air traffic, because it can stall plane engines (Lechner et al., 2018). It can also damage local crops, causing significant

economic losses in the agricultural sector. In some cases, it can have beneficial effects, acting as a fertilizer that enriches the soil with key elements for the proper development of C, N, S, and P cycles (Ciriminna et al., 2022). However, the fertilizing potential of volcanic ash depends on multiple factors, such as the weather conditions in the area, the amount of ash emitted, its composition, and the crop type (Mihai et al., 2023). The composition of the volcanic ash is also crucial in that it can trigger environmental problems, for example by contaminating water supplies by decreasing their pH and increasing their fluorine content (Stewart et al., 2006). Last but not least, pyroclastic flows can cause numerous fatalities and exposure to volcanic ash can lead to eye, skin, and respiratory tract problems, such as irritation, abrasion, conjunctivitis, coughing, and sore throats (Beylin et al., 2022).

The Canary Islands are part of the Canarian Volcanic Province (Spain), which is located off the northwestern coast of Africa, and consists of a group of volcanic islands and seamounts that follow a linear trend (León et al., 2019). This province originated from a hot spot combined with tectonic plate movement, which detaches the volcanoes from the magma source. Recent volcanic activity has been registered in

^{*} Corresponding author.

E-mail address: lopezm@ugr.es (M. López Gómez).

<https://doi.org/10.1016/j.clay.2024.107690>

Received 23 September 2024; Received in revised form 13 December 2024; Accepted 26 December 2024

Available online 31 December 2024

0169-1317/© 2024 Elsevier B.V. All rights are reserved, including those for text and data mining, AI training, and similar technologies.

the islands in the west of the archipelago, namely Lanzarote, Tenerife, and La Palma (Troll and Carracedo, 2016).

The eruption of the Tajogaite volcano, the youngest volcano on the island of La Palma, started on 19 September 2021. Volcanic activity was preceded by a seismic swarm and lasted until 13 December 2021. During this period, 200 million cubic meters of lava were emitted. In terms of volcanic ash, the Volcanology Institute of the Canaries (INVOLCAN, <https://www.involcan.org/>) reported that in the first 25 days of the eruption around 8–9 million cubic meters of ash and tephra were deposited. Currently, there are no clear laws or guidelines regarding the removal or recycling of ash. In fact, the European Union classifies this waste within “other municipal wastes” (20 03), and more specifically “street-cleaning residues” (20 03 03) (Commission notice 2018/C, 2018). As a result, the pyroclasts emitted during an eruption and deposited in inhabited areas or infrastructures (e.g., roads and airports) are usually disposed of in landfills. The environmental implications of such large amount of pyroclastic material mean that new disposal options must be explored.

The use of volcanic ash for construction purposes dates back to Ancient Rome, where a pozzolanic material from Pozzuoli (Naples, Italy) was mixed with lime to produce hydraulic mortars. The Romans inherited lime production techniques from the Greeks and the Etruscans, and enhanced them by adding pozzolana, volcanic sediments in which silicates and aluminosilicates react with the CaO in the presence of moisture to produce compounds with cementitious properties (Modena et al., 2018). Roman mortars are famous for their durability and their capacity to set underwater, which enabled buildings and cities to be erected in marine environments and allowed the Empire to expand across the Mediterranean Sea (Jackson et al., 2012). The use of volcanic ash in ancient building materials was not restricted to the manufacture of mortars, as volcanic temper from Somma-Vesuvius has also been found in ceramics from the *Cumae* archaeological site near Naples (Verde et al., 2022).

Nowadays volcanic ash has several possible uses (Lemoungna et al., 2018), including the manufacture of construction materials, lunar and Martian soil simulators, and soap abrasives (Dehn and McNutt, 2015). Within the field of construction materials, most of the research on volcanic ash has been devoted to geopolymers, lime and cement mortars. Barone et al. (2021) studied the use of volcanic ash from Etna to produce geopolymers, and found that, when cured at 100 and 400 °C, this product can be used as an alkali-activated material. For their part, Cavalieri et al. (2024) stated that the production of geopolymers using volcanic ash reduced CO₂ emission by up to 78 % compared to traditional concrete mortars. As regards the manufacture of mortars, Contraffatto (2017) highlighted that certain kinds of volcanic ash do not confer hydraulic properties on the mortar and can only be used as aggregates. In their review, Hamada et al. (2023) concluded that the addition of volcanic ash to concrete caused a denser matrix to develop, improving some of the mechanical properties and the durability of the resulting materials. Ahmad et al. (2023) highlighted the worsening of concrete flowability after volcanic ash was added to the mix, and the negative implications of employing very high doses of this additive. On the positive side, they also stressed that the addition of volcanic ash to concrete mortars helped reduce manufacturing costs. Martín-Rodríguez et al. (2024) tested the use of volcanic ash from La Palma in the production of blended and alkali cement and reported a reduction in the compressive strength of the final product.

Several reviews and studies have addressed the use of waste materials as additives in brick production (Al-Fakih et al., 2019; Dondi et al., 1997; Murmu and Patel, 2018; Zhang, 2013). These found, for example, that olive stones (López Gómez and Cultrone, 2023), paper pulp (Muñoz et al., 2020), and sawdust (Cultrone et al., 2020) usually increase the porosity and thermal insulation of the bricks. As regards the use of inorganic wastes, household glass has proven useful in increasing the compactness of fired samples (Hasan et al., 2020), while bricks made with added fly ash in proportions of up to 20 % had similar properties to

those made without additives (Eliche-Quesada et al., 2018). Finally, the use of diatomaceous earth increased the open porosity (Galán-Arboledas et al., 2017).

However, there is little available bibliography on the use of volcanic products. Gencil (2015) demonstrated that the addition of 10, 20, 30, and 40 % by weight of pumice to the clayey mix diminished the compressive strength of the resulting fired bricks, although they complied with the specifications for use as construction materials. Cobîrzan et al. (2021) obtained satisfactory results when using volcanic tuff from Romania in proportions of up to 30 % to produce fired bricks, concluding that the compressive resistance depended mainly on the firing temperature. For their part, Belfiore et al. (2024) tested the use of volcanic ash, together with chamotte, to produce ceramic tiles obtaining the best results when 10 % by weight of fine volcanic ash and 10 % of chamotte were added to the clayey material. Finally, Cultrone (2022) found that the addition of 10 and 20 % by weight of volcanic ash from Mount Etna (Italy) in the production of clay bricks enhanced their durability against salt attack. Although clayey earth is not an expensive material (17 \$/Tm, U.S. Geological Survey, 2023), it is a non-renewable natural resource. The incorporation of volcanic ash would reduce the high volume of the clayey material that needs to be extracted (13.000 kt/yr only in the USA), thereby reducing costs and preserving the environment.

These scarce bibliographical references on this topic represent the first attempts to reuse volcanic ash in the brick industry. With this in mind, this paper aims to provide a detailed study of the chemical, mineralogical and textural changes produced by the addition of volcanic ash from La Palma to bricks fired at different temperatures, focusing in particular on the influence of the amount and size of the particles added. To achieve these objectives, bricks were produced using three different percentages (10, 20 and 30 %) and two grain sizes (fine or coarse) of volcanic ash and were then compared with control samples made without this temper.

2. Materials and Methods

2.1. Raw materials

The clayey sediment used to make the bricks was provided by a ceramics company, Cerámica Castillo Siles, S.L., who quarried it from Pleistocene levels that outcrop in Viznar (Granada, Spain). The source area is part of the Granada Basin, which is located over the contact between the Internal and External Zones of the Betic Cordillera and is filled with detrital materials from the Neogene and Quaternary periods.

The volcanic ash from La Palma was provided by the Volcanology Institute of the Canaries (INVOLCAN), which is collecting the ash to study the magmatic processes related to the 2021 volcanic eruption. In general, the volcanic materials ejected after the eruption of the Tajogaite volcano are rich in Ti-augite, olivine, Ti-magnetite, amphibole and plagioclase (Pankhurst et al., 2022). After the ash was gathered, it was milled and sieved to obtain two granulometric fractions: one named “coarse” (G, $0.6 < \phi < 2$ mm) and the other “fine” (F, $\phi < 0.6$ mm). The upper limit for the grain size (2 mm) was selected in line with the study performed by Cultrone (2022), while the lower limit (0.6 mm) was chosen to enable us to observe the interaction between these smaller particles and the clay matrix under the microscope. 10, 20 and 30 % by weight of volcanic ash were added to the clayey material. These percentages were chosen because they had previously been used in research studies by Cobîrzan et al. (2021) and Cultrone (2022) that produced interesting results.

2.2. Manufacture of brick samples

18 bricks were manufactured with a volcanic ash temper and 3 were made with no additive, as control samples. The clayey sediment from Viznar, with and without volcanic ash was molded by hand with

kneading water and placed into wooden molds measuring $16 \times 12 \times 4$ cm. The mixture was flattened with a ruler to remove surface irregularities. After approximately 2 h, the bricks were demolded and cut into smaller samples ($4 \times 4 \times 4$ cm) with a stretched cotton thread. In total, 12 cubic samples were obtained from each mold and each brick type. The samples were air dried in the lab at approximately 18°C for three weeks before being fired in a Hobersal JM 22/16 electric oven.

The samples were fired at 800, 950, and 1100°C . 950°C was selected because the company that provided the raw materials for the study currently fires their bricks at this temperature, while the other two temperatures were chosen to enable us to study the mineralogical and textural changes that take place at lower and higher temperatures. Table 1 offers a summary of the characteristics of the fired samples and their labels.

During the firing process, the dried samples were first heated at 100°C for an hour to remove any possible remaining moisture. The temperature was then increased by $3^\circ\text{C}/\text{min}$ until the desired firing temperature was reached, after which it was kept constant for 3 h. Subsequently, the oven was switched off and the samples were removed the next day to enable slow cooling and avoid the formation of fractures due to the β -to- α quartz transition at 573°C (Knappek et al., 2016). After removal from the oven, the bricks were immersed in water to prevent the sample breaking due to the possible presence of CaO grains, a phenomenon known as “lime blowing” (Laird and Worcester, 1956).

2.3. Characterization of raw materials and brick samples

X-Ray Fluorescence (XRF) was used to determine the major elements in the raw materials (clayey sediment and volcanic ash) and the fired bricks. The analyses were performed using a PANalytical Zetium spectrometer with a Rh anode and a 4 kV X-Ray generator. The calibration was performed with a set of over thirty certified geological standards (Govindaraju, 1994).

To study the possible release of chemical elements from the bricks into the water, leaching tests were performed. Samples without volcanic ash and those with 30 % of temper were powdered and mixed with deionized water in a ratio of 1:2 (sample:water). The samples were placed in graduated centrifuge tubes and placed on a Nahita blue orbital shaker model 685/2 at 160 rpm for 24 h before being centrifuged in a Kubota 2000 apparatus to extract the water fraction. To stabilize the

Table 1

Firing temperature ($T^\circ\text{C}$), weight percentage (wt%), grain size and nomenclature of the samples prepared. Legend: F: fine grain size ($\phi < 0.6$ mm); G: coarse grain size ($0.6 < \phi < 2$ mm).

T $^\circ\text{C}$	Temper		Samples' acronyms
	wt%	Grain size	
800	0		B800
	10	F	B(10F)800
		G	B(10G)800
	20	F	B(20F)800
		G	B(20G)800
	30	F	B(30F)800
G		B(30G)800	
950	0		B950
	10	F	B(10F)950
		G	B(10G)950
	20	F	B(20F)950
		G	B(20G)950
	30	F	B(30F)950
G		B(30G)950	
1100	0		B1100
	10	F	B(10F)1100
		G	B(10G)1100
	20	F	B(20F)1100
		G	B(20G)1100
	30	F	B(30F)1100
G		B(30G)1100	

solution, 0.1 ml of nitric acid was added per each 5 ml of water. The same procedure was followed to prepare leachates of unheated volcanic ash (Ash) and ash heated at 1100°C (Ash₁₁₀₀). In addition, a blank sample was prepared using only deionized water and the same percentage of nitric acid. The concentration of Be, Sc, V, Cr, Mn, Co, Ni, Cu, Zn, As, Y, Mo, Cd, Sn, Sb, Ba, Tl, Pb, Bi, Th, U was analyzed using inductively coupled plasma mass spectrometry (ICP-MS) with a NexION 300D (Perkin Elmer) spectrometer. Rh was used as an internal standard. Precision was better than $\pm 5\%$ for an analyte concentration of 10 ppm. The Geochemical Earth Reference Model (GERM) partition coefficient database (<https://earthref.org/KDD-old/>) was used to interpret the results.

A PANalytical X'Pert Pro X-Ray Diffractometer was used to identify the minerals that make up the clayey sediment, the volcanic ash, and the fired bricks. The samples were ground in an agate mortar to a particle size of less than $53\ \mu\text{m}$. They were then analyzed by X-Ray Diffraction (XRD) using the randomly oriented powder method. The measurements were performed under the following conditions: $\text{CuK}\alpha$ ($\lambda = 1.5405\ \text{\AA}$) radiation, 45 kV voltage, 40 mA current, $4\text{--}70^\circ$ 2θ exploration range, and 0.1° $2\theta/\text{s}$ goniometer speed. To study the influence of high firing temperature on the mineralogy of the volcanic ash, a few grams of fine ash ($\phi < 0.6$ mm) were heated at 1100°C for 3 h and studied by XRD under the same working conditions as above. To determine the mineralogy of the clayey sediment in more detail, oriented aggregates were prepared by removing the carbonates with an acetic acid solution (CH_3COOH) before adding sodium hexametaphosphate ($\text{Na}_6\text{P}_6\text{O}_{18}$) and centrifuging the samples in a Kubota 2000 apparatus. These aggregates were then studied air dried (OA_AD), solvated with ethylene glycol for 24 h (OA_EG) and heated at 550°C for 90 min (OA_550). Quantitative analysis of the fired bricks was carried out by adding 20 % of zincite (ZnO) as an internal standard and homogenizing the sample with an agate mortar. For these measurements the goniometer speed was lowered to 0.01° $2\theta/\text{s}$. The diffractograms obtained were interpreted using Profex 5.2.4 and HighScore v.4.8. software.

The thermal decomposition of the clayey sediment was assessed by means of thermogravimetry (TG) and Differential Scanning Calorimetry (DSC). A Mettler-Toledo TGA/DSC1 was used for the analysis, and the sample was heated from 25 to 950°C at a rate of $20^\circ\text{C}/\text{min}$ in a flowing air atmosphere.

The granulometry of the clayey sediment was determined using the Robinson's pipette method (Soil Conservation Service (USDA), 1972). The fine fraction of the volcanic ash was measured with a Malvern Instruments Mastersizer 2000LF apparatus that uses laser diffraction, and the coarse fraction was measured using an ASTM 18 sieve. The results of the granulometric analyses were plotted on a Winkler diagram (Winkler, 1954) in order to determine the suitability for brick production of the clayey raw material with and without added volcanic ash. The plasticity of the clayey sediment without temper and with the addition of 10, 20, and 30 % by weight of both grain sizes of volcanic ash was studied using Casagrande's liquid limit device following the UNE-EN ISO 17892-12 (2019) standard. The results were plotted on a Bain-Higley diagram (Bain and Higley, 1979) to determine whether the addition of volcanic ash impaired or enhanced brick production.

To study the texture and the mineralogy of the bricks with and without volcanic ash, thin sections were prepared and studied under two microscopes. A CarlZeiss Jenapol-U polarized optical microscope coupled with a Nikon D7000 digital camera was used to obtain images of the texture with plane-polarized (PPL) and cross-polarized light (XPL). In addition, unheated and heated (at 1100°C) volcanic ash fragments and two polished thin sections of bricks with coarse volcanic ash (the largest fragments) fired at 800 and 1100°C were carbon coated and observed at higher magnification with a Phenom XL Desktop Scanning Electron Microscopy (SEM), equipped with an EDS detector.

3. Results and Discussion

3.1. Characterization of the raw materials

The XRF results are presented in Table 2. The clayey sediment from Viznar (V) and the volcanic ash from La Palma (Ash) have similar percentages of SiO₂, Al₂O₃ and CaO, although these oxides are produced by the different minerals they contain. Ash, whose mineralogy will be described later on, is richer in Fe, Mg, Na, and Ti. The volcanic ash did not undergo Loss on Ignition (LOI), while the 15 % rate detected in the clay from Viznar may be due to the presence of carbonates, organic matter, and phyllosilicates that release CO₂ and OH when heated.

As regards the mineralogy, the diffractogram of the clayey sediment (Fig. 1a) indicates the presence of phyllosilicates (mainly illite/muscovite type), carbonates (calcite and dolomite), feldspars *s.l.*, and quartz. The presence of calcite and dolomite explains the significant percentages of CaO (12.6 %) and MgO (4.3 %) detected by XRF. The analysis of the clay fraction revealed the presence of smectite due to its swelling capacity, which caused a displacement of the *d*₀₀₁ peak from 12.67 Å to 16.41 Å after the oriented aggregate had been solvated with ethylene glycol (see the inset in Fig. 1a). Another phyllosilicate detected was paragonite, which is not a common phase but is frequently found in certain sediments from southeastern Spain (Martin Garcia et al., 1997). The presence of both phases was signaled by a double-peak in the kaolinite and chlorite positions in V_{AD}. At 550 °C some of these peaks disappeared or were less intense after heating, due to the decomposition of kaolinite and the dehydroxylation of chlorite. However, the chlorite *d*₀₀₁ peak at 14 Å remained visible and was more intense (Moore and Reynolds Jr., 1997).

The result of the thermogravimetric analysis (TG-DSC) of the clayey material from Viznar is shown in Fig. 1b. The initial endothermic peaks at 92 and 140 °C are due to the loss of hygroscopic water. The peak at 252 °C corresponds to the combustion of the organic matter in the soil, whereas the peaks at 345 and 489 °C are caused by the dehydroxylation of phyllosilicates. The main weight loss (i.e., 13.3 %) is due to the decomposition of carbonates and the release of CO₂ that starts around 700 °C and ends at 810 °C. Above this temperature, the curve shows a slight weight loss owing to a further dehydroxylation of muscovite-type phyllosilicates (Lecomte et al., 2007). The weight loss during this test (16.03 %) was similar to that obtained by XRF (Table 2, LOI, 15.16 %).

Fig. 2 shows the X-ray diffraction pattern of the unfired volcanic ash (Ash) in which Ca-rich plagioclase, olivine, titanomagnetite, and clinopyroxene are identified. Given the paragenesis of the volcanic rocks from La Palma, the clinopyroxene could correspond to augite (Pankhurst et al., 2022). All these minerals are responsible for the high Fe₂O₃, MgO and Na₂O contents detected by XRF (Table 2). The diffractogram for the volcanic ash heated at 1100 °C (Ash₁₁₀₀) reveals the decomposition of olivine and titanomagnetite and the formation of hematite. In Ash₁₁₀₀ an increase in the intensity of the peaks pertaining to plagioclase and clinopyroxene can be observed, although the involvement of amorphous silica in the formation of these phases is uncertain. A reduction of the background noise can also be observed in sample Ash₁₁₀₀.

Fig. 3 presents polarized optical microscope images of the volcanic ash. Fig. 3a shows the abundance of round-shaped pores generated by gas release during the volcanic eruption. Some of these pores can also be distinguished by the naked eye reaching approximately 2 mm in size. Subhedral kaersutite and euhedral augite phenocrystals can also be seen in Fig. 3a, though the pyroxene is far more abundant than the amphibole. Augite was identified by XRD as clinopyroxene but kaersutite

could not be identified using this technique due to its very low content in the sample. A basal section of kaersutite can be seen in Fig. 3b, as well as a plagioclase crystal, which was too small to enable us to identify the exact type of plagioclase; however, considering the type of rock and the XRD results, it is probably a calcium plagioclase. Opaque crystals can also be observed in the sample, which according to XRD results could correspond to magnetite (Fig. 3c). Large olivine phenocrystals are also found, albeit in small numbers (Fig. 3d).

Fig. 4 shows SEM images of the unfired volcanic ash (Ash, a and b) and of the ash fired at 1100 °C (Ash₁₁₀₀, c and d). Fig. 4c shows how the volcanic ash particles self-aggregate during the heating process, increasing in size, while new phases seem to crystallize on their surface, leaving it rougher (Fig. 4d).

The Atterberg limits for the raw material from Viznar with and without the addition of volcanic ash are listed in Table 3. As expected, the addition of volcanic ash reduced both the Liquid Limit (LL) and the Plastic Limit (PL). In general, the higher the volcanic ash content, the greater the reduction. This is because part of the clayey soil is replaced by an aplastic material, reducing its ability to absorb water.

When the results for the Plastic Limit (PL) and Plasticity Index (PI) are plotted in a Bain-Highley diagram (Fig. 5a), we can see that the addition of volcanic ash to the clayey sediment from Viznar makes the resulting paste unsuitable for manufacturing bricks with an extruder. The samples plotted furthest away from the “acceptable extrusion” area are those with 20 and 30 % of coarse volcanic ash and 30 % of fine volcanic ash. By contrast, the samples with 10 % of fine volcanic ash are very close to the required values.

Fig. 5b plots the granulometry of the clayey sediment from Viznar without and with the addition of 10, 20 and 30 wt% of volcanic ash in the Winkler diagram, which evaluates the suitability of the raw materials for brick production. The Viznar clayey sediment is suitable for perforated brick production, although it borders on the roof tiles field. After the addition of volcanic ash, the raw material moves diagonally towards the bottom right of the diagram, such that those made with 10 wt% of volcanic ash fall within the field of perforated bricks, while those made with 20 and 30 wt% fall within that of solid bricks (Fig. 5b). The use of coarse or fine grain ash makes little difference as the values almost overlap, although the samples made with fine grain ash (F, $\phi < 0.6$ mm) were positioned slightly to the left of those made with coarse ash (G, $0.6 < \phi < 2$ mm).

3.2. Macroscopic observation, chemical and mineralogical composition of bricks

After firing, the ash particles in the bricks fired at 1100 °C turned red, while those fired at 800 and 950 °C maintained their black tone. This chromatic change was studied in detail under a digital videomicroscope (DVM, Leica DVM 2000). A detailed observation of the brick surface showed that the samples fired at 800 °C presented a reddish matrix in which irregular pores (Fig. 6a) and black volcanic ash fragments (Fig. 6b) could be distinguished. The matrix of the samples fired at 950 °C was also red and with irregular pores (Fig. 6c), although some areas of the volcanic ash fragments had turned brownish (Fig. 6d). By contrast, the samples fired at 1100 °C had more rounded pores and a light-yellow matrix (Fig. 6e). At this temperature, most volcanic ash particles underwent a color change from black to red, although some dark areas could still be observed in several fragments (Fig. 6f).

With respect to the chemical composition of the fired bricks (Table 4), there were no significant differences between the samples in

Table 2

Chemical composition (in %) of the volcanic ash (Ash) and the clayey sediment from Viznar (V). LOI stands for loss on ignition.

Sample	SiO ₂	Al ₂ O ₃	Fe ₂ O ₃	MnO	MgO	CaO	Na ₂ O	K ₂ O	TiO ₂	P ₂ O ₅	LOI	Total
Ash	43.81	13.65	12.95	0.18	7.99	11.11	3.67	1.57	3.62	0.77	0.00	99.32
V	45.17	13.32	4.89	0.06	4.33	12.63	0.64	2.38	0.69	0.12	15.16	99.39

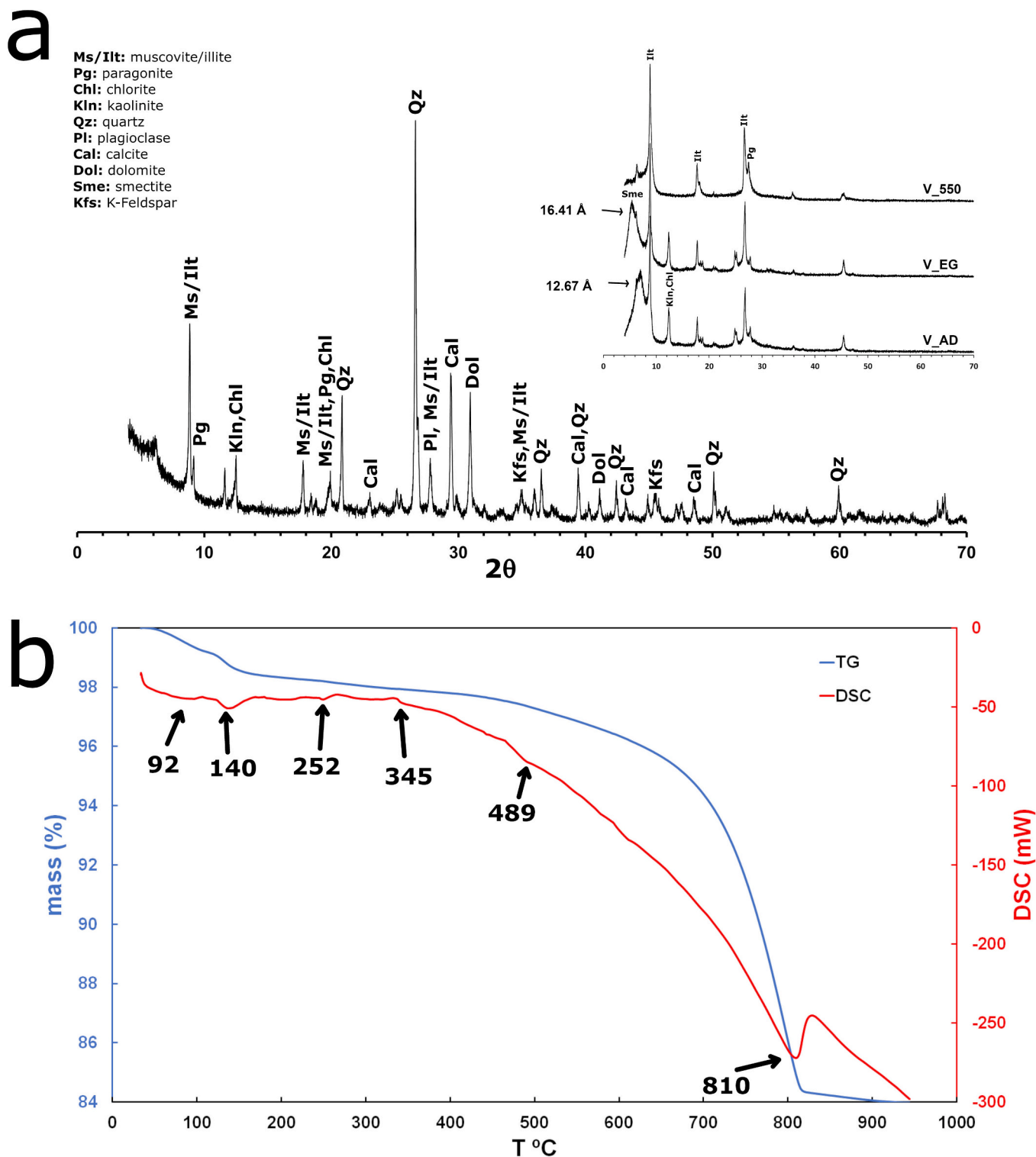


Fig. 1. (a): Diffractogram of the clayey sediment from Viznar. Mineral abbreviations suggested by Warr (2021). The following oriented aggregates can be seen in the inset: air dried (V_AD), treated with ethylene glycol (V_EG) and heated at 550 °C (V_550). (b): Thermogravimetry (TG, blue) and Differential Scanning Calorimetry (DSC, red) curves for the clayey sediment from Viznar.

terms of the percentages of the main oxides. The only discrepancy was in the LOI, which was approximately 10 % lower than the value obtained for the clayey sediment and fell as the firing temperature rose from 800 to 1100 °C. This is due to the further dehydroxylation of phyllosilicates and the release of CO₂ from the carbonates that were still present in the fired bricks. This phenomenon was mitigated by the increase in the

percentage of volcanic ash, due to the smaller proportion of clayey sediment in the mixture and, consequently, of carbonates and phyllosilicates. By contrast, the addition of volcanic ash increases the Fe, Mg, Na, and Ti contents in the bricks, because of the higher percentages of these elements in the ash.

Regarding the mineralogical composition of the fired samples, at

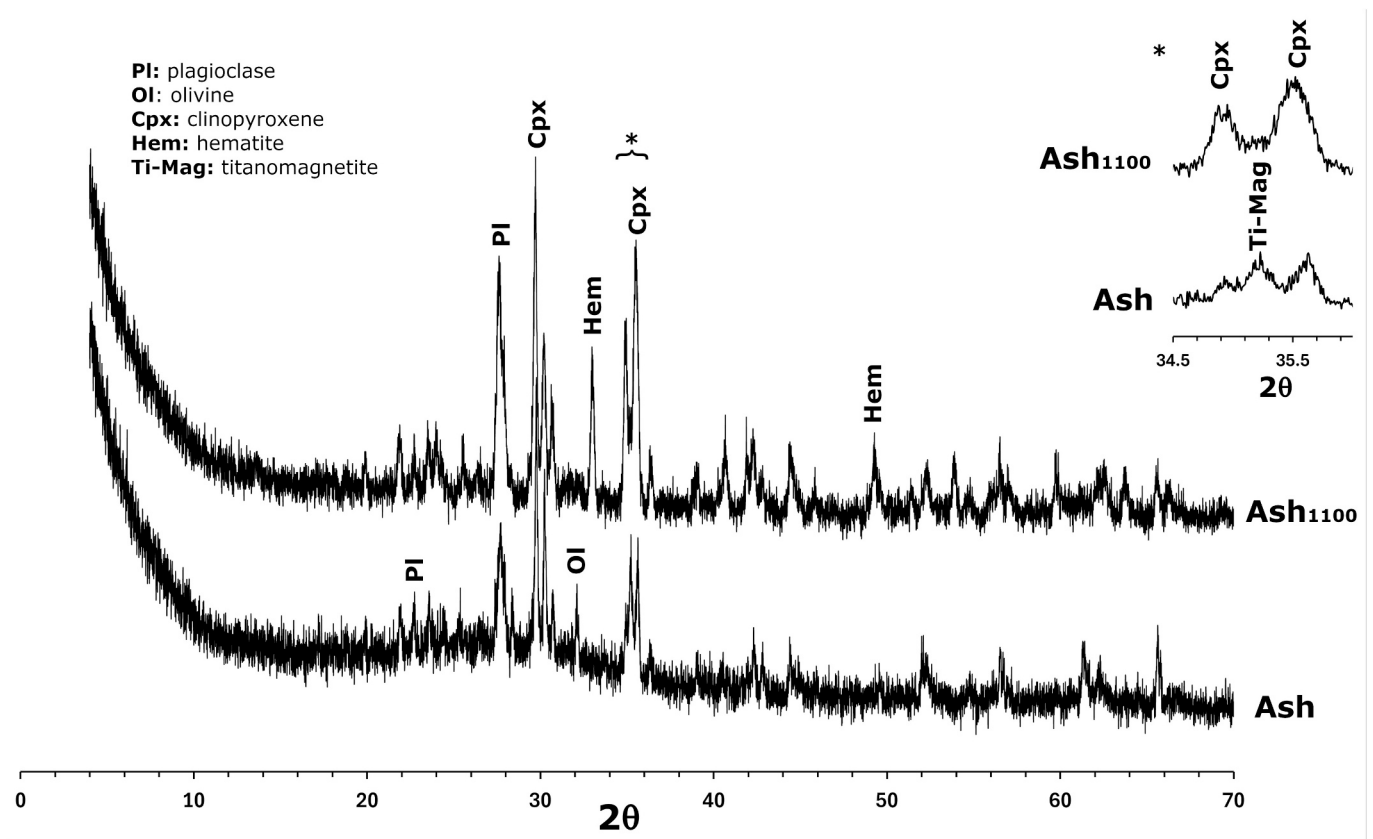


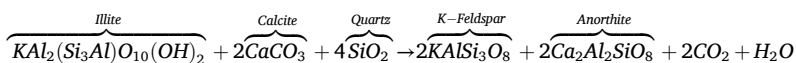
Fig. 2. Diffractogram for the unfired volcanic ash (Ash) and the volcanic ash heated at 1100 °C (Ash₁₁₀₀). Mineral abbreviations suggested by Warr (2021). Upper right: magnified section of the diffractogram with the peak for titanomagnetite (Ti-Mag).

800 °C the phyllosilicates such as smectite, chlorite and kaolinite disappear except for illite/muscovite and paragonite. At this temperature, calcite is still present, unlike dolomite. This is related to the decomposition of these carbonates, a process described below (see Section 3.4). At 950 °C, the calcite and paragonite peaks are no longer detectable and the peaks for illite/muscovite are lower. The Ca released during the decomposition of the carbonates recombines with Si to form a new phase, gehlenite (Ca₂Al₂SiO₇). At 1100 °C, the illite/muscovite peak is no longer visible and a new phase, diopside (CaMgSi₂O₆), crystallizes combining Ca and Mg from the calcite and dolomite with Si from the quartz (Cultrone et al., 2001) (Fig. 7). The addition of volcanic ash causes augite to be detected but does not seem to favor the development of new mineral phases during firing. In the bricks fired at 800 °C, the addition of ash leads to a reduction in the intensity of the illite/muscovite, quartz, and calcite peaks, owing to the fact that smaller amounts of clayey sediment were used in the manufacture of these

in the samples with added volcanic ash fired at this temperature.

Table 5 shows the results of the quantitative XRD analysis. For the samples without temper, the percentage of quartz falls progressively as firing temperature increases, especially between 950 °C and 1100 °C when it slumps from 28.8 % to 20 %. The increase in temperature also entails a decrease in muscovite/illite and a progressive increase in plagioclase, K-Feldspar and amorphous material.

The increase in amorphous material is due to the progressive vitrification of the bricks. The increase in the amount of K-Feldspar as firing temperature increases is related to the K and Si released after the decomposition of muscovite/illite, together with the decomposition of quartz and other silicates. Something similar takes place in the formation of Ca-rich plagioclases with the Ca produced by the decomposition of the carbonates (Cultrone et al., 2001):



samples. Similarly, in the samples fired at 950 and 1100 °C, less gehlenite was formed in the samples with volcanic ash than in those without it. By contrast, the diopside (cpx, Fig. 7) peaks in the bricks with volcanic ash fired at 1100 °C appear to be higher than those for the control sample. This is because the formation of this phase is overestimated by the presence of augite from the volcanic ash, as most peaks for the two minerals overlap. This means that the more generic term of clinopyroxene must be used when referring to possible augite and diopside peaks

If we look at how the percentage of volcanic ash influences the mineralogy of the bricks, the increase in ash content progressively decreases the percentage of quartz, muscovite/illite and gehlenite, while increasing that of the amorphous phase. The higher the percentage of volcanic ash, the lower the clay content, and therefore of these minerals. For its part, the volcanic glass is responsible for the increase in amorphous material. The amount of augite (cpx, Table 5), originally present in the volcanic ash, increases progressively in line with the ash content

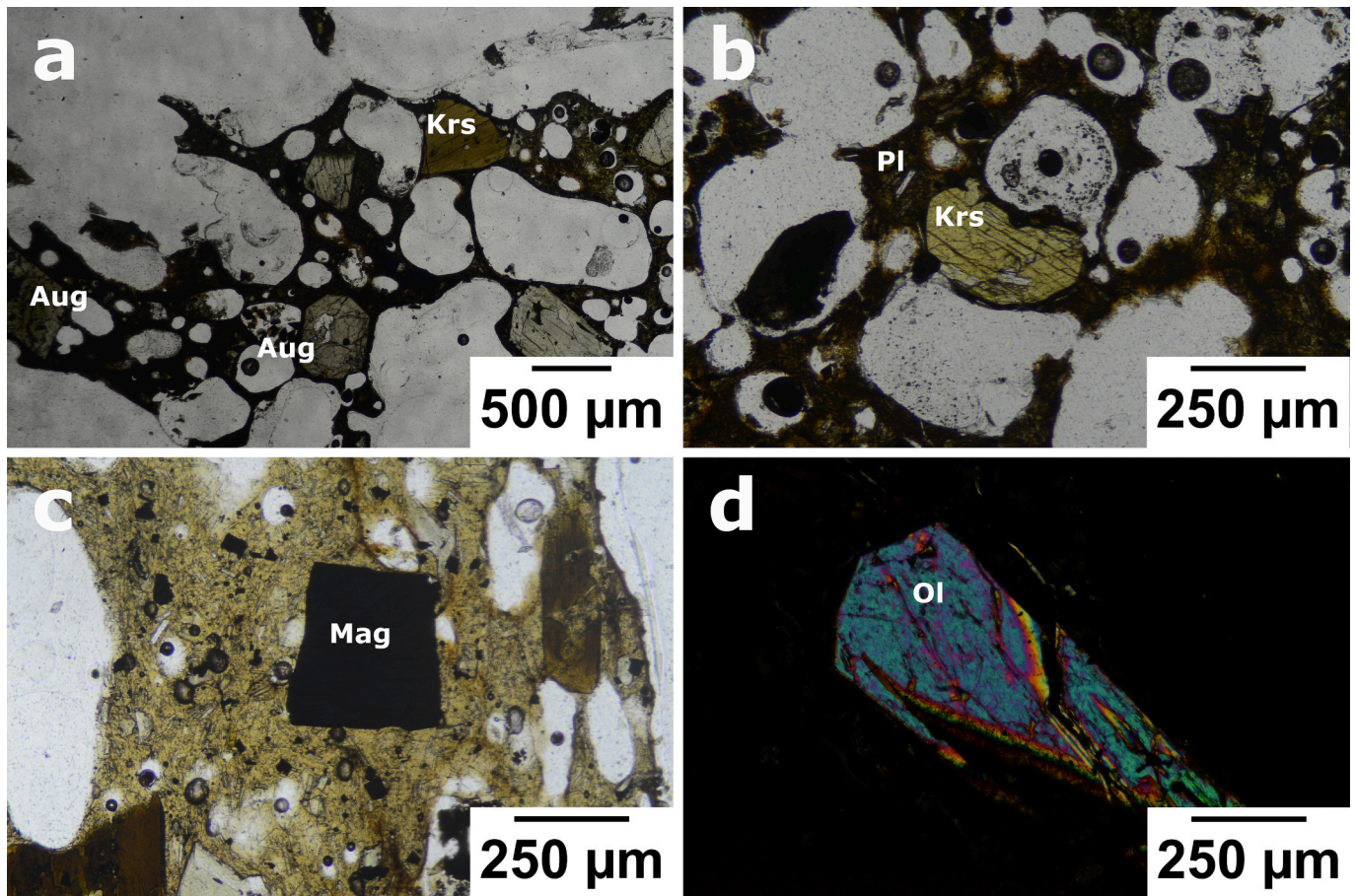


Fig. 3. Polarized optical microscopy images of volcanic ash fragments. a: porous vitreous matrix with phenocrystals of augite and kaersutite (PPL). b: basal section of an amphibole and small plagioclase crystals (PPL). c: opaque xenomorphic crystal, probably magnetite (PPL). d: olivine crystal (XPL).

for the samples fired at 800 and 950 °C. However, at 1100 °C the overlap of the augite peaks with those for diopside, makes it difficult to estimate the amount for each one of these clinopyroxenes.

3.3. Release of chemical elements

Fig. 8 shows the results of the leaching test. The concentrations of all the different elements are below the specified contamination limits for industrial soils in the Andalusian region (CMAJA, 1999): As (300 mg/kg), Cd (30 mg/kg), Co (400 mg/kg), Cr (1000 mg/kg), Cu (1000 mg/kg), Mo (500 mg/kg), Ni (750 mg/kg), Pb (2000 mg/kg), Sn (500 mg/kg), Tl (30 mg/kg), and Zn (3000 mg/kg). When the volcanic ash is added to the fired bricks, most of the element concentrations are below the limits set for irrigation by the Food and Agriculture Organization (FAO, <https://www.fao.org/>), except for V, Cr and Mo. However, surface runoff would dilute these elements before reaching the urban drainage system. In addition, although different leaching procedures are used, all the element concentrations are below the US EPA toxicity characteristic contamination thresholds for hazardous waste (Code Of Federal Regulations, 2012).

The elemental concentration of the leachates from the fired bricks is very low except for V, Cr, Mo and Ba. It seems that the concentration of these elements is related to the firing temperature rather than the temper content or grain size. By contrast, the leachates obtained from the volcanic ash on its own (Ash and Ash₁₁₀₀) show high V, Mn, Cu, As, Mo, and Ba concentrations.

The XRD showed that heating the volcanic ash leads to the decomposition of olivine and magnetite and the formation of hematite. The leaching test has demonstrated that heating the volcanic ash increases

the V and As content, slightly increases that of Mo and Ba and slightly diminishes that of Mn and Cu. This is due to the compatibility of the elements, in other words, their tendency to be concentrated in the solid phase during melting or crystallization (White, 2020). V is compatible for magnetite (Tourrette et al., 1991), an oxide which is usually associated with As (Alvarez and Carol, 2019). The decomposition of magnetite could therefore have led to the release of V and As.

Regarding the brick leachates, the percentage of clayey sediment used to produce the bricks was always higher than that of volcanic ash, which explains the importance of firing temperature in the elemental distribution. V, Cr, Mo, and Ba are linked to the phyllosilicate, muscovite (Bosazza, 1940; Dubacq and Plunder, 2018; Randive et al., 2015; Zheng et al., 2017), whose decomposition during firing could release them. In addition, the maximum Cr concentration is observed in the bricks fired at 950 °C, whereas in those fired at 1100 °C this element appears in lower concentrations. This behavior can be explained by the incorporation into the diopside of Cr, an element that is compatible with clinopyroxenes (Shepherd et al., 2022).

3.4. Petrographic features and microchemical transformations

Fig. 9 shows the texture of the bricks under optical microscopy. Fig. 9a highlights a gneiss and a partially decomposed carbonate fragment in a brick fired at 800 °C. Carbonates have lost their typical birefringence and appear grey-colored with crossed polars. The gneiss fragments are usually elongated in one direction and measure about 500 μm in length, although some fragments of more than 1 mm can also be seen. Serpentine fragments were identified in all the samples, although they did not appear in sufficient quantities to enable any minerals from

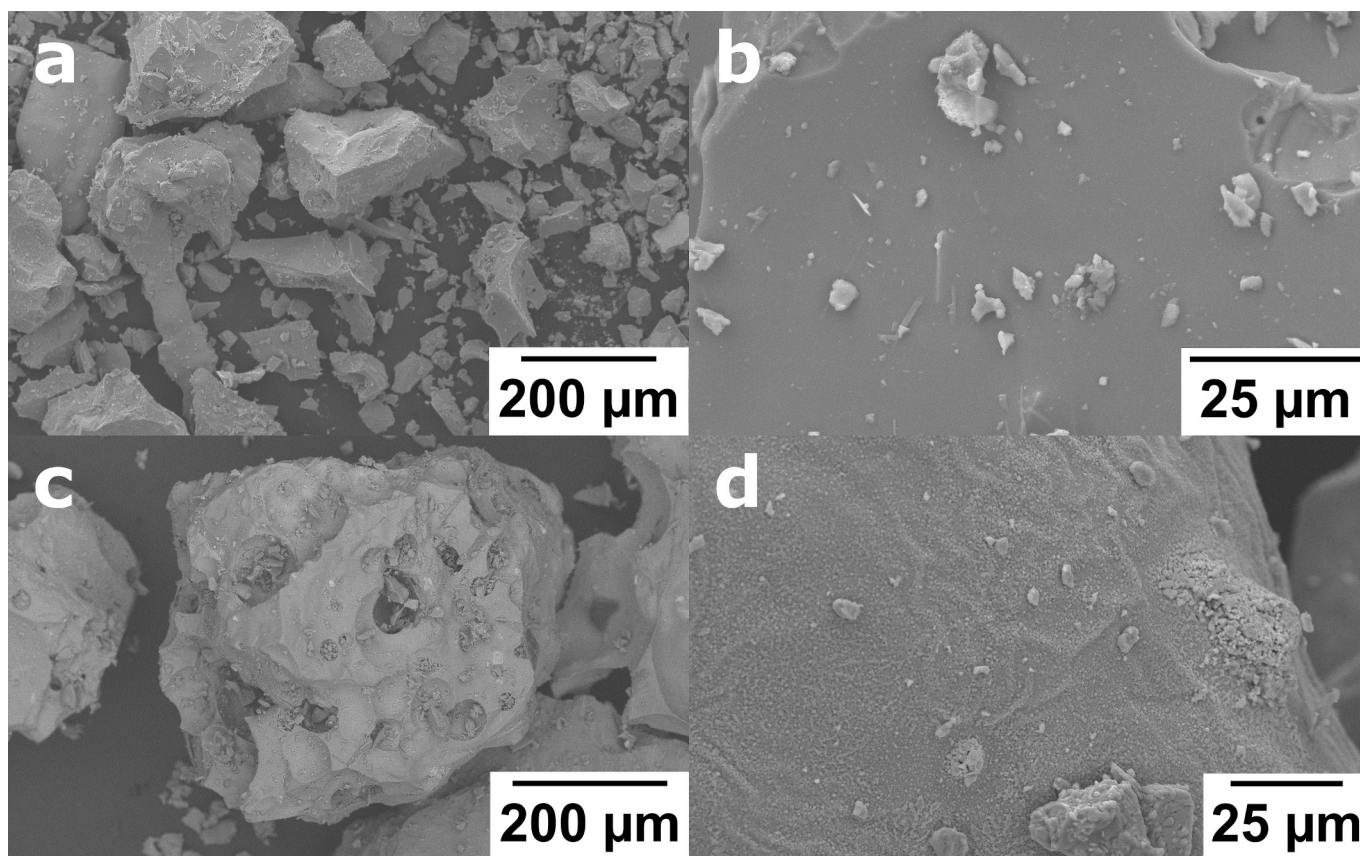


Fig. 4. Electron microscopy images of unfired ash fragments (a and b) and of ash fragments fired at 1100 °C (c and d).

Table 3

Liquid Limit (LL), Plastic Limit (PL) and Plasticity Index (PI) of the clayey sediment from Viznar without volcanic ash (V) and with the addition of 10, 20 and 30 % of fine (F) and coarse (G) volcanic ash.

Sample	LL	PL	PI
V	28.50	17.79	10.71
F10	25.52	15.82	9.70
F20	24.35	13.27	11.08
F30	20.35	14.21	6.14
G10	24.98	17.36	7.62
G20	21.68	17.25	4.43
G30	20.68	15.43	5.25

the serpentine group to be detected by XRD (Fig. 9b). These fragments are usually elongated in shape and their longest axis measures around 600 μm . Gneiss and serpentinite fragments are very common the sediments from the Granada Basin (Hughes, 1995). The fragments of volcanic ash and their characteristic round-shaped pores are easily distinguishable in the samples with added temper (Fig. 9c). No signs of reaction between the volcanic ash and the surrounding matrix are visible at this temperature. At 950 °C some of the volcanic ash fragments have reddish parts (Fig. 9d). This finding is consistent with the macroscopical observations and is linked to the incipient formation of hematite within these grains. While the olivine crystals in the samples fired at 800 and 950 °C appear intact (Fig. 9e), an incipient alteration in the crystal edges can be observed in those fired at 1100 °C (Fig. 9f), which is coherent with the results obtained by XRD.

As regards the texture of the samples, the bricks fired at 800 °C have smaller, more irregular pores than those fired at 1100 °C because of the vitrification of the matrix. It is also important to highlight that the addition of coarse volcanic ash leads to an increase in porosity (Fig. 9g). This is because the volcanic ash has isolated pores and its use as an

additive causes an increase in the porosity of the clayey mix. This phenomenon is less noticeable in bricks with fine volcanic ash because the fragments are smaller (Fig. 9h). In addition, at the optical microscopy scale, the apparent lack of reaction between the temper and the brick matrix results in a poor bond between these two materials. This could increase porosity, especially for the bricks made with coarse volcanic ash and fired at low temperatures, in that at 1100 °C, the ash is partially melted and there is a better link with the clay matrix. Finally, under the microscope at 1100 °C, a color change can be observed in the brick matrix with and without ash, which turns dark due to vitrification.

Fig. 10 contains various SEM images of the samples with coarse volcanic ash fired at 800 and 1100 °C. The matrix of the brick fired at 800 °C (Fig. 10a) contains carbonates, quartz, phyllosilicates and gneiss fragments, which could also be identified with the optical microscope. At this temperature, the quartz and phyllosilicates remain unaltered and the carbonate fragments are still recognizable, although they have started to decompose. Fig. 10a shows a dolomite grain edge that is rich in Ca compared to the center of the crystal. Galai et al. (2007) reported that the decomposition of dolomite leads to the formation of a dolomite core, surrounded by a Ca-rich layer, which in turn is surrounded by a Mg layer. This is consistent with the presence of a dark core which is surrounded first by a light layer and then by a dark layer in the dolomite crystal (Fig. 10a). Regarding the matrix of the bricks fired at 1100 °C, some new oval pores have formed between the phyllosilicate sheets, due to the release of gases (Fig. 10b). White dots that correspond to hematite can also be identified between these sheets. The matrix of the bricks fired at this temperature is highly vitrified, which improves the interconnectivity between the grains and makes the pores and the grain surfaces smoother. In Fig. 10b, iron oxides crystals can also be observed in the glassy phase of the brick matrix. However, these very small crystals are not enough to maintain the red color of the bricks, which instead turn yellow to the naked eye (see Fig. 6). This is because the

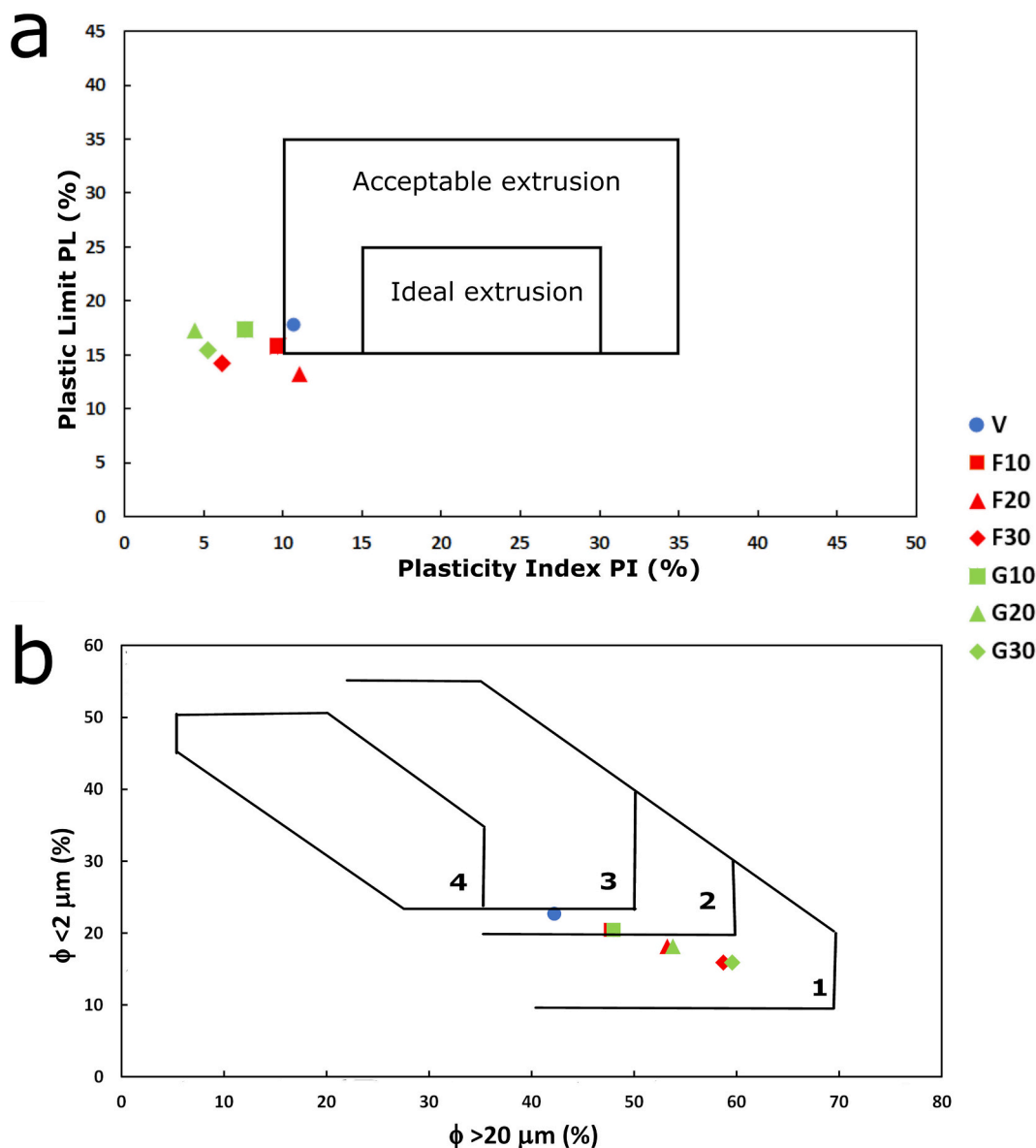
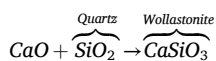


Fig. 5. Bain-Highley (a) and Winkler diagrams (b). Blue circle: clayey sediment from Viznar; square: clayey sediment after the addition of 10 % of volcanic ash; triangle: clayey sediment with 20 % of volcanic ash; diamond: clayey sediment with 30 % of volcanic ash. The symbols in red refer to samples made with fine volcanic ash, while those in green are for the coarse ash samples. The different fields in the diagrams cover the samples suitable for making: 1 = solid bricks; 2 = perforated bricks; 3 = roof tiles; 4 = thin-walled hollow bricks. (For interpretation of the references to color in this figure legend, the reader is referred to the web version of this article.)

incorporation of Fe into the lattice of the Ca-aluminosilicates formed during firing at high temperatures in calcareous clay bricks hampers the formation of iron oxides (Maniatis et al., 1981; Kreimeyer, 1987). The quartz fragment edges identified in this sample react with carbonates to form wollastonite (Fig. 10c) as follows (Cultrone et al., 2001):



The presence of this phase in XRD was doubtful, and its scarcity in the brick sample makes its peaks difficult to identify.

As far as the mineralogical and textural features of the volcanic ash are concerned, the titanomagnetite in the ash fired at 800 °C shows initial stages of exsolution, with lamellae formation (Fig. 10d), although the composition of these lamellae could not be determined. At 1100 °C, the exsolution of titanomagnetite is more evident (Fig. 10e) and leaves two phases, one rich in Mg and Al (dark grey) and the other rich in Ti (white). According to Arguin et al. (2018) Mg^{2+} and Al^{3+} can

respectively substitute the Fe^{2+} and Fe^{3+} in the titanomagnetite ($\text{Fe}^{2+}(\text{Fe}^{3+}, \text{Ti})_2\text{O}_4$) structure. When this mineral exsolves it forms ilmenite ($\text{Fe}^{2+}\text{Ti}^{4+}\text{O}_3$) and pleonaste ($(\text{Mg}, \text{Fe})\text{Al}_2\text{O}_4$) (Tan et al., 2016), seen respectively as white and dark grey in Fig. 10. At 800 °C the olivine crystals in the volcanic ash are unaltered (Fig. 10f), while at 1100 °C the olivine is surrounded by iron oxides (white dots) and presents intergrowths of two phases, one light grey and the other white (Fig. 10g), which may correspond to magnetite and pyroxene. The formation of magnetite and pyroxene symplectites in olivine was described by Ashworth and Chambers (2000) and Moseley (1984) and is due to the presence of ferric iron. The Fe^{3+} in the olivine forms magnetite and the rest of the elements are incorporated into the pyroxene structure. In addition, at 1100 °C the Fe in the olivine tends to diffuse to the edges of the crystal (Mackwell, 1992), leading to the formation of iron oxides (Fig. 10g).

Finally, as regards the contact between the brick matrix and the volcanic ash, at 1100 °C the brick matrix is adhered to the ash due to

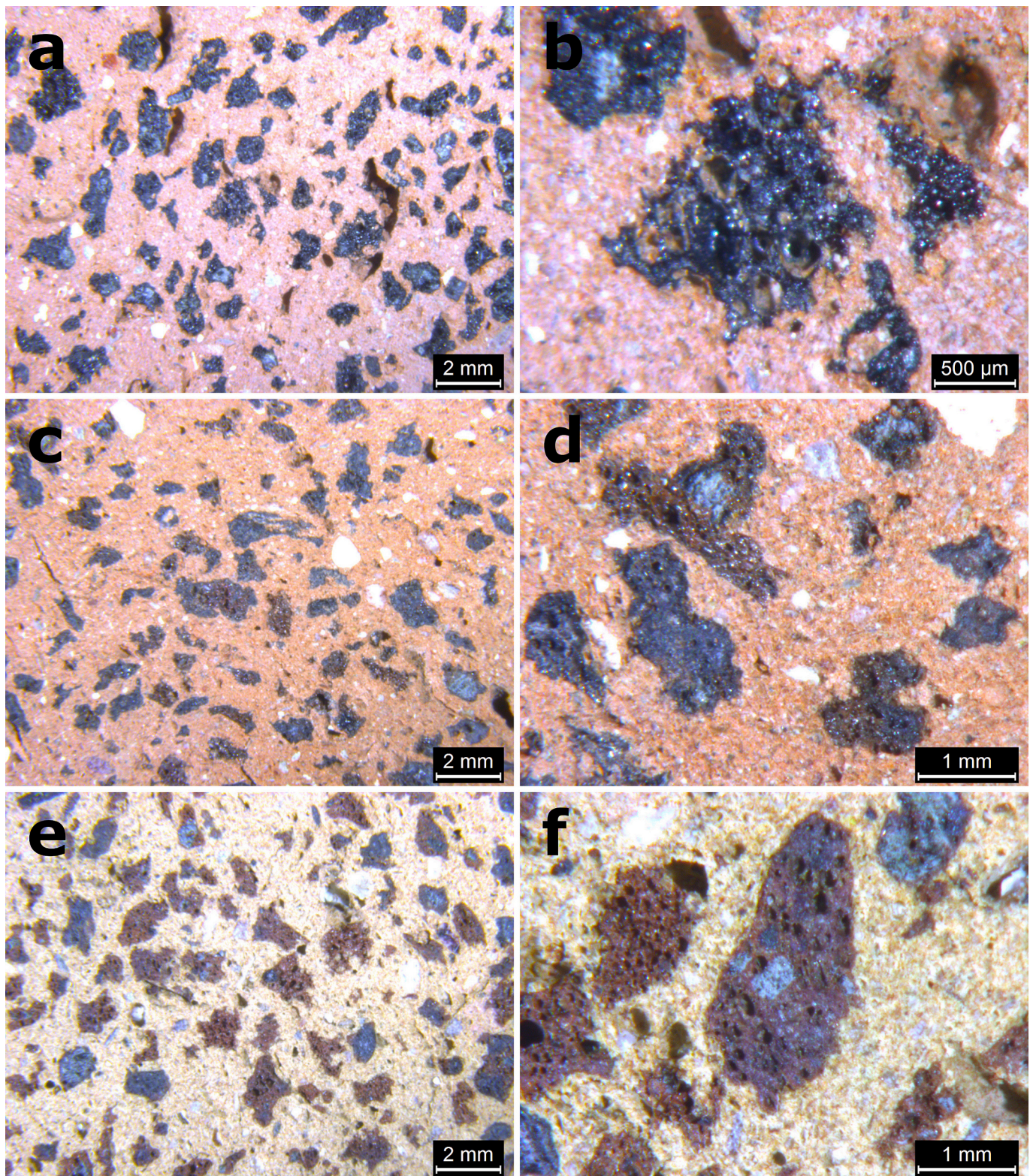


Fig. 6. General view (a, c, e) and detailed DVM images (b, d, f) of the bricks with coarse volcanic ash fired at 800 °C (a and b), 950 °C (c and d), and 1100 °C (e and f).

vitriification (Fig. 10h). At this temperature, the ash particles partially melt, so enhancing their bond with the clay matrix. This makes it harder to distinguish the separation between the volcanic ash and the brick matrix than at 800 °C (Fig. 10f). Additionally, some iron oxide crystals which are not present at 800 °C are identified in the volcanic glass in the bricks fired at 1100 °C (Fig. 10h).

4. Conclusions

The large volumes of volcanic ash generated by a volcanic eruption mean that new reuse options must be found so as to avoid the accumulation of this waste material in landfills. The use of volcanic ash as an additive in the manufacture of fired bricks reduces the volume of clayey

Table 4
Chemical composition (in %) of the fired brick samples. LOI stands for loss on ignition.

Sample	SiO ₂	Al ₂ O ₃	Fe ₂ O ₃	MnO	MgO	CaO	Na ₂ O	K ₂ O	TiO ₂	P ₂ O ₅	LOI	Total
B800	51.59	15.20	5.44	0.07	4.90	13.20	0.75	2.73	0.75	0.14	4.77	99.54
B950	52.36	15.42	5.55	0.07	5.19	13.92	0.75	2.77	0.76	0.14	2.70	99.63
B1100	53.92	15.74	5.72	0.08	5.04	14.23	0.77	2.66	0.74	0.14	0.59	99.63
B(10F)800	50.79	14.97	6.37	0.09	5.44	13.10	1.07	2.58	1.08	0.21	3.93	99.63
B(10F)950	52.00	15.36	6.52	0.09	5.58	13.59	1.08	2.64	1.09	0.21	1.44	99.60
B(10F)1100	52.71	15.41	6.56	0.09	5.45	13.56	1.12	2.66	1.13	0.22	0.67	99.58
B(10G)800	49.67	14.48	6.19	0.09	5.24	12.68	1.06	2.50	1.08	0.21	6.35	99.55
B(10G)950	51.71	15.27	6.50	0.09	5.55	13.70	1.09	2.61	1.10	0.21	1.82	99.65
B(10G)1100	53.07	15.32	6.45	0.09	5.45	13.54	1.09	2.66	1.09	0.21	0.70	99.67
B(20F)800	50.14	14.80	7.17	0.10	5.68	13.06	1.38	2.46	1.39	0.27	3.02	99.47
B(20F)950	50.31	15.01	7.25	0.10	5.84	13.11	1.39	2.47	1.41	0.28	2.53	99.70
B(20F)1100	51.49	15.16	7.38	0.10	5.98	13.44	1.40	2.44	1.44	0.28	0.59	99.70
B(20G)800	48.60	14.25	6.84	0.09	5.63	13.40	1.26	2.30	1.31	0.25	5.63	99.56
B(20G)950	50.90	15.14	7.34	0.10	5.80	12.80	1.41	2.51	1.42	0.28	1.85	99.55
B(20G)1100	51.50	15.25	7.46	0.10	5.91	13.33	1.44	2.43	1.44	0.29	0.55	99.70
B(30F)800	48.77	14.54	7.98	0.11	6.08	12.41	1.66	2.31	1.68	0.34	3.73	99.61
B(30F)950	50.01	14.95	8.15	0.11	6.13	12.84	1.72	2.37	1.72	0.34	1.23	99.57
B(30F)1100	50.46	14.77	8.23	0.11	6.28	13.08	1.67	2.25	1.73	0.35	0.75	99.68
B(30G)800	49.24	14.63	8.02	0.11	6.06	12.45	1.71	2.34	1.69	0.34	2.99	99.58
B(30G)950	49.74	14.86	8.25	0.11	6.22	12.93	1.75	2.34	1.75	0.36	1.28	99.59
B(30G)1100	50.32	14.76	8.19	0.11	6.25	13.24	1.73	2.31	1.76	0.36	0.52	99.55

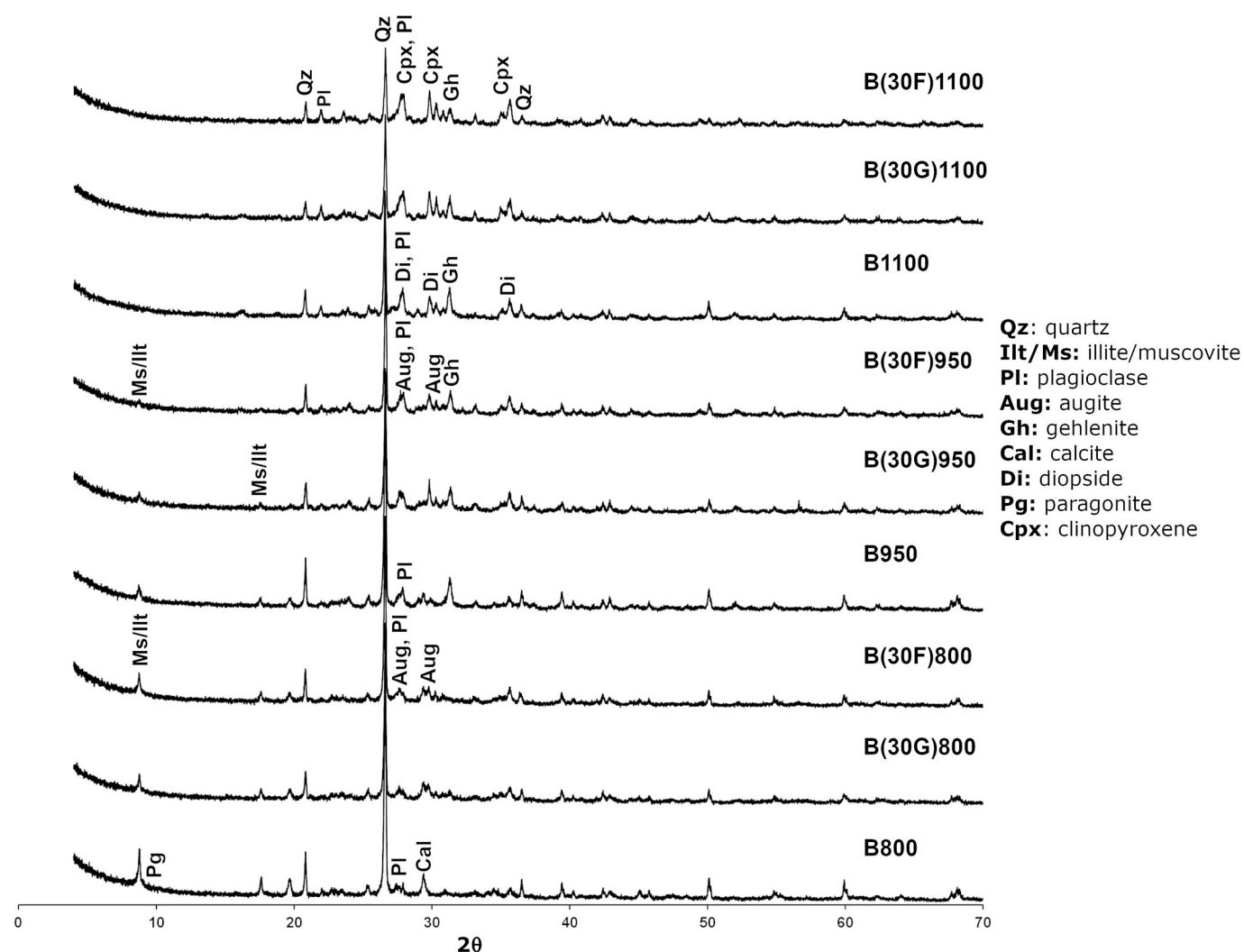


Fig. 7. Diffractograms of the samples without temper and with 30 % of coarse and fine grain volcanic ash fired at 800, 950, and 1100 °C. Mineral abbreviations suggested by Warr (2021).

Table 5

Mineral phases (calculated with Profex) and amorphous material (Am, calculated with HighScore) percentages. Abbreviations suggested by Warr (2021): qz: quartz; ilt/ms: illite/muscovite; cal: calcite; pl: plagioclase; san: sanidine; gh: gehlenite; cpx: clinopyroxene. * newly formed diopside is added to this value.

Sample	Qz	Ms/Ilt	Cal	Na-Pl	Ca-Pl	K-Fsp	Gh	Cpx	Am
B800	29.04	24.46	4.24	2.49	–	2.28	–	–	35.12
B(10G)800	26.45	21.37	5.03	0.58	4.04	3.00	–	1.12	44.25
B(10F)800	24.94	19.10	4.29	0.82	4.65	1.88	–	2.08	39.12
B(20G)800	22.44	19.91	4.78	1.50	4.14	2.76	–	3.02	55.25
B(20F)800	24.42	19.89	4.25	2.36	4.55	1.92	–	3.98	54.63
B(30G)800	18.66	16.77	4.68	1.37	3.79	2.49	–	10.23	51.75
B(30F)800	20.18	15.56	4.27	1.37	2.49	2.52	–	10.79	60.37
B950	28.80	13.95	–	2.67	9.04	3.95	9.00	–	50.75
B(10G)950	25.10	11.41	–	5.54	7.68	4.02	10.86	7.63	58.75
B(10F)950	25.97	11.02	–	6.48	8.42	2.64	8.20	5.77	61.37
B(20G)950	23.24	11.46	–	3.70	9.42	1.39	7.02	8.37	65.50
B(20F)950	22.27	9.17	–	2.24	10.55	0.94	6.87	9.53	58.25
B(30G)950	19.17	8.99	–	4.31	8.09	1.20	5.87	12.03	62.25
B(30F)950	16.49	9.76	–	3.29	9.38	0.54	6.74	14.31	64.62
B1100	20.00	–	–	–	27.77	4.04	8.35	14.17*	60.75
B(10G)1100	19.04	–	–	–	30.67	2.35	6.55	21.93*	67.75
B(10F)1100	19.75	–	–	–	32.18	2.85	5.25	20.09*	69.75
B(20G)1100	15.29	–	–	–	31.01	1.36	4.16	19.82*	71.87
B(20F)1100	15.17	–	–	–	30.17	2.77	3.90	22.58*	70.75
B(30G)1100	11.62	–	–	–	31.36	1.69	3.27	22.44*	75.62
B(30F)1100	12.31	–	–	–	28.72	2.16	2.71	19.65*	71.50

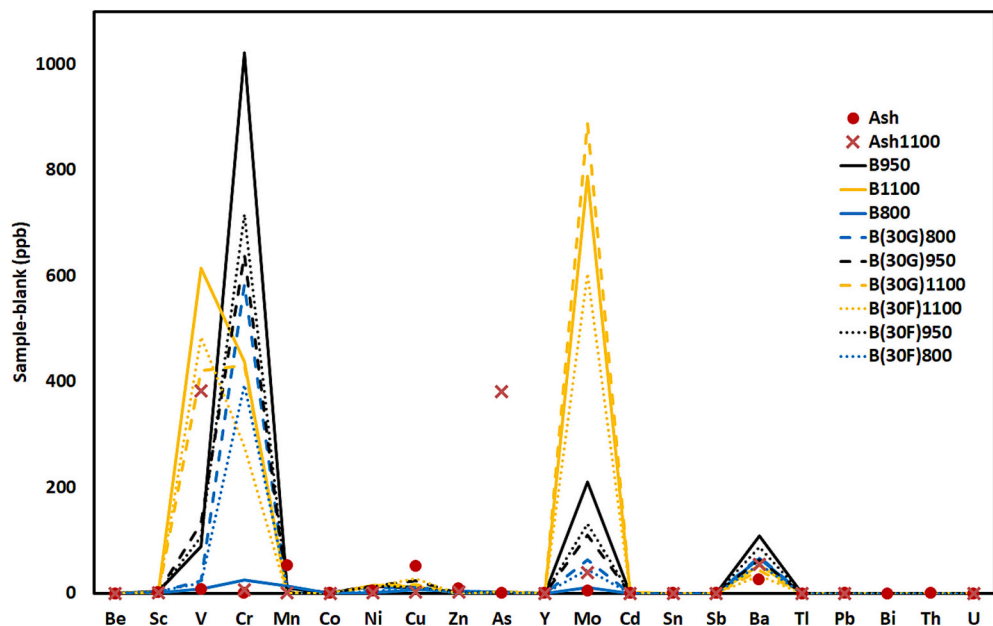


Fig. 8. Composition of the leachates from the samples. Red dots: unheated volcanic ash; red crosses: volcanic ash heated at 1100 °C; blue: bricks fired at 800 °C; black: bricks fired at 950 °C; yellow: bricks fired at 1100 °C. The solid line represents the bricks with no additive, the dashed line represents the bricks with fine volcanic ash and the dotted line represents those with coarse volcanic ash. (For interpretation of the references to color in this figure legend, the reader is referred to the web version of this article.)

sediment necessary to produce the brick, which reduces manufacturing costs, and offers new options for the disposal of this waste.

The addition of volcanic ash did not lead to the formation of new mineral phases in the brick matrix. In fact, no reactions between the volcanic ash and the surrounding brick matrix were observed. In the samples with volcanic ash, a reduction was observed in some of the phases originally present in the clayey sediment (phyllosilicates, quartz, and calcite) or formed during firing (gehlenite and diopside). In addition, augite, an inosilicate present in the volcanic ash but not in the clayey sediment, was also identified in the diffractograms for the bricks made with added temper. In fact, the higher the percentage of temper added, the greater the reduction in the phyllosilicates, quartz, calcite, diopside, and gehlenite, and the higher the percentage of augite. The grain size of the volcanic ash had no effect on the percentages of each

mineral in the bricks made with ash. The volcanic ash in the samples fired at over 950 °C turned red in color due to the formation of iron oxides in the ash. At 1100 °C, the olivine exsolves to pyroxene and magnetite and the titanomagnetite exsolves to ilmenite and pleonaste. The elemental concentration of the fired bricks leachates is more related to the firing temperature than to the percentage or grain size of the volcanic ash and is below the established contamination limits for industrial soils in Andalusia. As regards the texture, the volcanic ash has abundant rounded pores and when it is added to the brick, it seems to increase its porosity, especially for the coarse temper. In addition, a better bond between the brick matrix and the ash was observed in the samples fired at 1100 °C. This is because the vitreous phase formed at this temperature adheres to the ash, which begins to melt.

This research has provided new data about the reactions that take

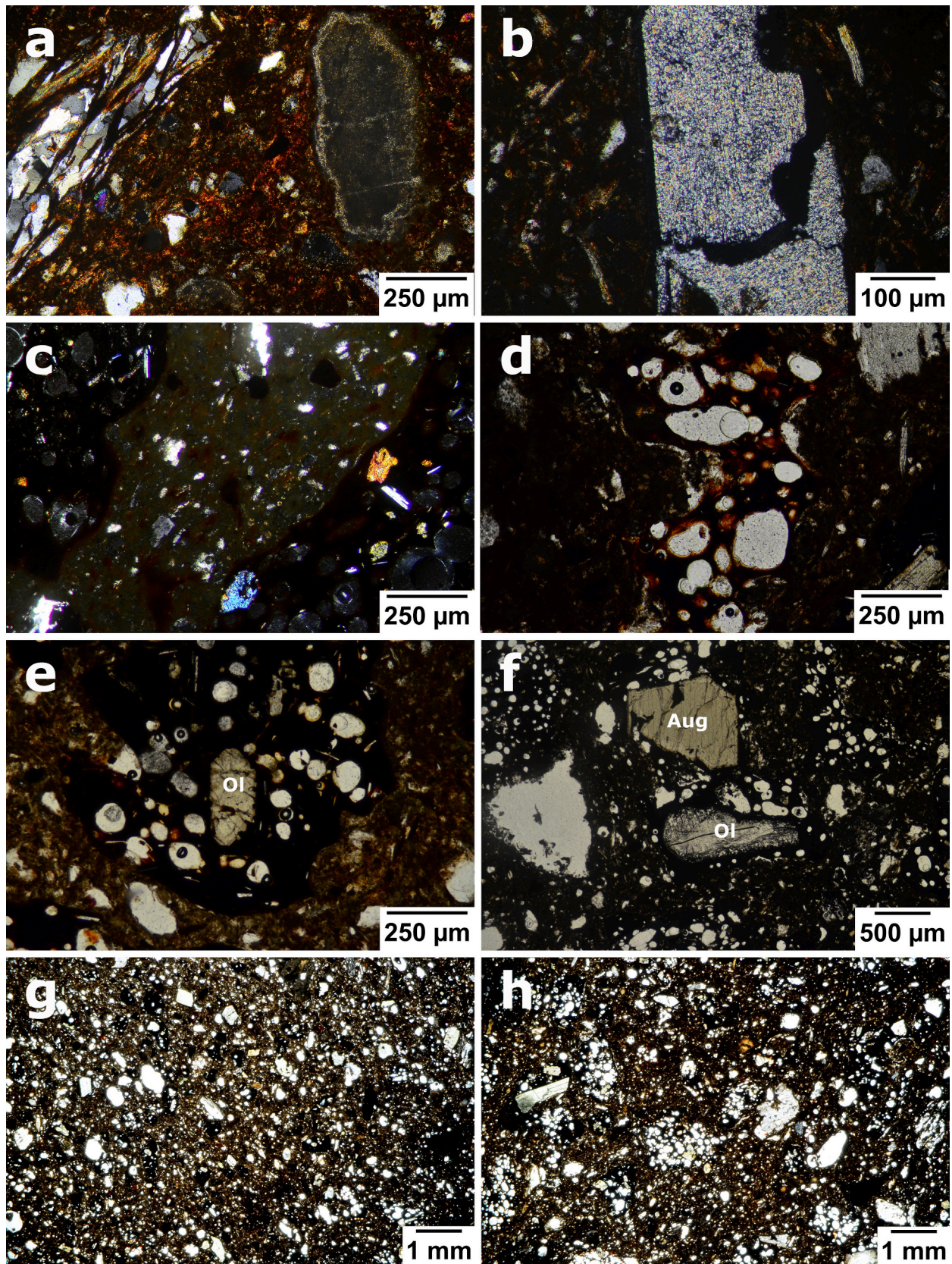


Fig. 9. Polarized optical images of the fired brick samples. a: calcite crystal and gneiss fragment fired at 800 °C (B800, XPL). b: serpentinite fragment (B950, XPL). c: coarse volcanic ash fragment in a brick fired at 1100 °C (B(30F)1100, XPL); d: volcanic ash fragment fired at 950 °C in which Fe oxides have formed (B950(30G), PPL); e: non-altered olivine crystal in a brick fired at 950 °C; f: altered olivine crystal in a brick fired at 1100 °C. g: brick with coarse volcanic ash fired at 950 °C (B(30G)950, PPL); h: brick with fine volcanic ash fired at 950 °C (B(30F)950, PPL).

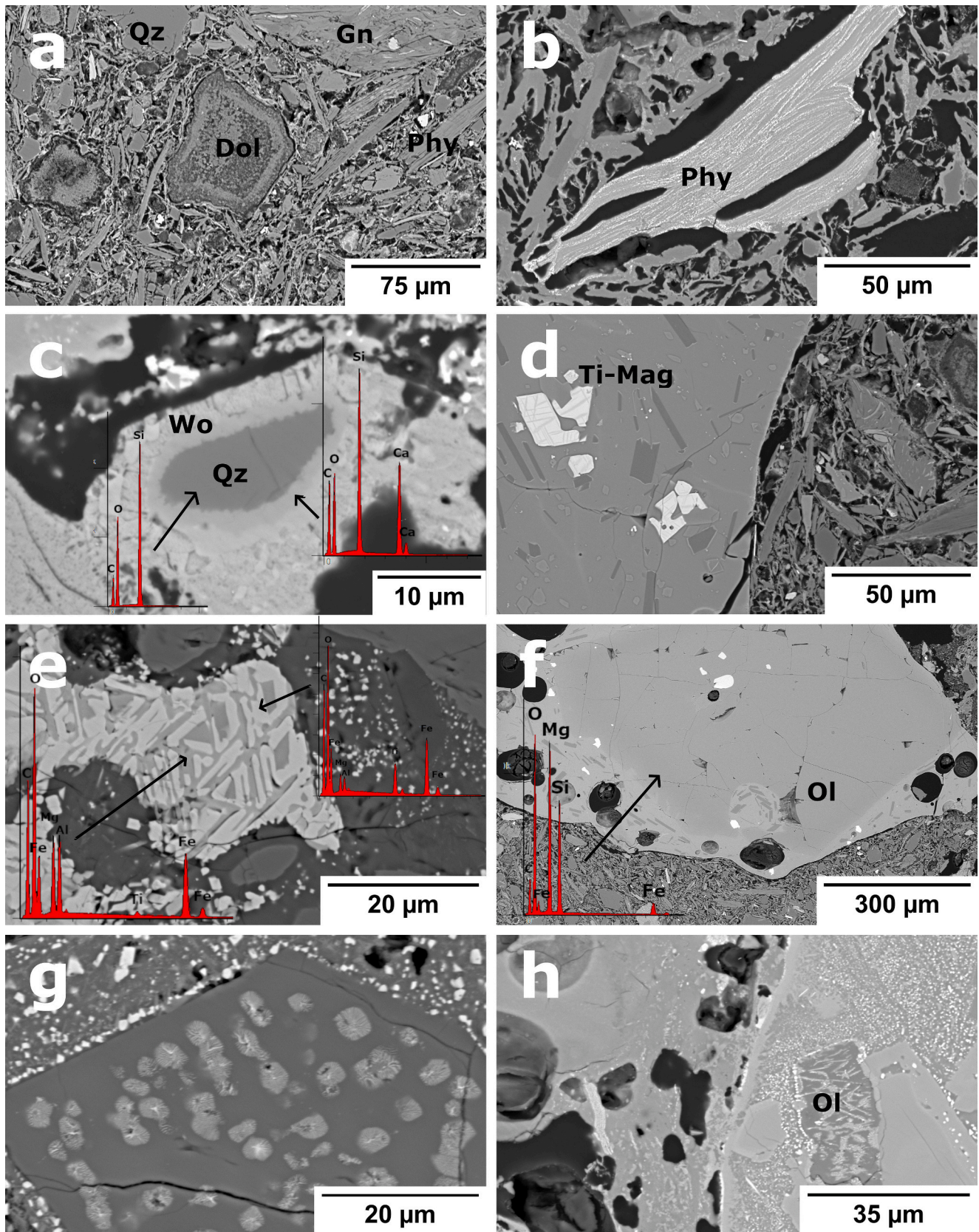


Fig. 10. SEM images and EDS analyses of samples with coarse volcanic ash fired at 800 and 1100 °C. a: dolomite (Dol), quartz (Qz), phyllosilicate (Phy) and gneiss (Gn) fragments in a brick fired at 800 °C. b: phyllosilicate fragment fired at 1100 °C. c: quartz (Qz) altered to wollastonite (Wo) at 1100 °C. d: contact between the brick matrix (right) and the volcanic ash (left) with a partially exsolved titanomagnetite at 800 °C. e: titanomagnetite totally exsolved to pleonaste and ilmenite. f: olivine (Ol) fragment in volcanic ash at 800 °C. g: pyroxene and magnetite symplectites in an olivine fired at 1100 °C and surrounded by iron oxides. h: contact between the brick matrix (left) and the volcanic ash (right) at 1100 °C.

place in fired bricks when volcanic ash is used as an additive. It also offers a detailed study of the changes in the mineral composition and percentages during firing and sheds light on the influence of the grain size of the volcanic ash and the firing temperature on the texture of the fired bricks. Further research needs to be conducted to evaluate how the addition of volcanic ash affects the physical and mechanical properties of the fired bricks and assess the susceptibility to decay of bricks made with this temper compared to those made without it.

Funding

This study was funded by the Junta de Andalucía Research Group RNM179 and the Ministry of Science and Innovation under the Research Project PID2020-119838RA-I00.

CRediT authorship contribution statement

María López Gómez: Methodology, Investigation, Formal analysis, Data curation, Writing – original draft. **Giuseppe Cultrone:** Supervision, Investigation, Funding acquisition, Formal analysis, Conceptualization, Writing – review & editing.

Declaration of competing interest

The authors declare that they have no known competing financial interests or personal relationships that could have appeared to influence the work reported in this paper.

Data availability

Data will be made available on request.

Acknowledgments

We would like to thank Cerámica Castillo Siles for providing the raw material used to prepare the bricks and the Centro de Instrumentación Científica of the University of Granada for its assistance with the XRF analyses. The manuscript has benefited from reviews by three anonymous referees.

References

- Ahmad, J., Althoey, F., Abuhussain, M.A., Deifalla, A.F., Özkılıç, Y.O., Rahmawati, C., 2023. Durability and microstructure analysis of concrete made with volcanic ash: a review (Part II). *Sci. Eng. Compos. Mater.* 30. <https://doi.org/10.1515/secm-2022-0211>.
- Al-Fakih, A., Mohammed, B.S., Liew, M.S., Nikbakht, E., 2019. Incorporation of waste materials in the manufacture of masonry bricks: an update review. *J. Build. Eng.* 21, 37–54. <https://doi.org/10.1016/j.job.2018.09.023>.
- Alvarez, M. Del P., Carol, E., 2019. Geochemical occurrence of arsenic, vanadium and fluoride in groundwater of Patagonia, Argentina: sources and mobilization processes. *J. S. Am. Earth Sci.* 89, 1–9. <https://doi.org/10.1016/j.jsames.2018.10.006>.
- Arguin, J.-P., Pagé, P., Barnes, S.-J., Girard, R., Duran, C., 2018. An Integrated Model for Ilmenite, Al-Spinel, and Corundum Exsolutions in Titanomagnetite from Oxide-Rich Layers of the Lac Doré complex (Québec, Canada). *Minerals* 8, 476. <https://doi.org/10.3390/min8110476>.
- Ashworth, J.R., Chambers, A.D., 2000. Symplectic Reaction in Olivine and the Controls of Intergrowth Spacing in Symplectites. *J. Petrol.* 41, 285–304. <https://doi.org/10.1093/ptrology/41.2.285>.
- Bain, J.A., Highley, D.E., 1979. Regional Appraisal of Clay Resources - a Challenge to the Clay Mineralogist. In: Mortland, M.M., Farmer, V.C. (Eds.), *Developments in Sedimentology, International Clay Conference 1978*. Elsevier, pp. 437–446. [https://doi.org/10.1016/S0070-4571\(08\)70741-6](https://doi.org/10.1016/S0070-4571(08)70741-6).
- Barone, G., Finocchiaro, C., Lancellotti, I., Leonelli, C., Mazzoleni, P., Sgarlata, C., Strocio, A., 2021. Potentiality of the use of Pyroclastic Volcanic Residues in the production of Alkali Activated Material. *Waste Biomass Valor.* 12, 1075–1094. <https://doi.org/10.1007/s12649-020-01004-6>.
- Belfiore, C.M., Parisi, S., Menta, S., Mazzoleni, P., 2024. Use of volcanic ash and chamotte as substitute temper in the production of ceramic tiles. *Appl. Clay Sci.* 262, 107603. <https://doi.org/10.1016/j.clay.2024.107603>.
- Beylin, D., Mantal, O., Haik, J., Kornhaber, R., Cleary, M., Neil, A., Harats, M., 2022. Soft tissue-related injuries sustained following volcanic eruptions: an integrative review. *Burns* 48, 1727–1742. <https://doi.org/10.1016/j.burns.2021.09.008>.
- Bosazza, V., 1940. Occurrence of Vanadium and Molybdenum in Clays. *Nature* 146, 746. <https://doi.org/10.1038/146746a0>.
- Cavaliere, M., Ferrara, P.L., Finocchiaro, C., Martorana, M.F., 2024. An Economic Analysis of the use of Local Natural Waste: Volcanic Ash of Mt. Etna Volcano (Italy) for Geopolymer Production. *Sustainability* 16, 740. <https://doi.org/10.3390/su16020740>.
- Ciriminna, R., Scurria, A., Tizza, G., Pagliaro, M., 2022. Volcanic ash as multi-nutrient mineral fertilizer: Science and early applications. *JSFA Rep.* 2, 528–534. <https://doi.org/10.1002/jsf2.87>.
- CMAJA, 1999. Los criterios y estándares para declarar un suelo contaminado en Andalucía y la metodología y técnicas de toma de muestra y análisis para su investigación. <http://www.ugr.es/~fjmartin/Criterios%20y%20estandares.pdf.04.11.2014>.
- Cobîrzan, N., Thalmaier, G., Balog, A.-A., Constantinescu, H., Ceclan, A., Nasui, M., 2021. Volcanic Tuff as secondary Raw Material in the production of Clay Bricks. *Materials* 14, 6872. <https://doi.org/10.3390/ma14226872>.
- Code Of Federal Regulations, 2012. Section 261.24 – Toxicity Characteristics. In: 40. US Government Printing Office.
- Commission notice 2018/C, 2018. 124/01 on technical guidance on the classification of waste, n.d., OJ C 124, 9.4.2018, pp. 1–134.
- Contrafatto, L., 2017. Recycled Etna volcanic ash for cement, mortar and concrete manufacturing. *Constr. Build. Mater.* 151, 704–713. <https://doi.org/10.1016/j.conbuildmat.2017.06.125>.
- Cultrone, G., 2022. The use of Mount Etna volcanic ash in the production of bricks with good physical-mechanical performance: Converting a problematic waste product into a resource for the construction industry. *Ceram. Int.* 48, 5724–5736. <https://doi.org/10.1016/j.ceramint.2021.11.119>.
- Cultrone, G., Rodríguez-Navarro, C., Sebastián, E., Cazalla, O., de la Torre, M.J., 2001. Carbonate and silicate phase reactions during ceramic firing. *Eur. J. Mineral.* 13, 621–634. <https://doi.org/10.1127/0935-1221/2001/0013-0621>.
- Cultrone, G., Aurrekoetxea, I., Casado, C., Arizzi, A., 2020. Sawdust recycling in the production of lightweight bricks: how the amount of additive and the firing temperature influence the physical properties of the bricks. *Constr. Build. Mater.* 235, 117436. <https://doi.org/10.1016/j.conbuildmat.2019.117436>.
- Dehn, J., McNutt, S.R., 2015. Chapter 74 - Volcanic Materials in Commerce and Industry. In: Sigurdsson, H. (Ed.), *The Encyclopedia of Volcanoes, Second edition*. Academic Press, Amsterdam, pp. 1285–1294. <https://doi.org/10.1016/B978-0-12-385938-9.00074-2>.
- Dondi, M., Marsigli, M., Fabbri, B., 1997. Recycling of industrial and urban wastes in brick production: a review. *Tile & Brick Int.* 13 (3), 218–225.
- Dubacq, B., Plunder, A., 2018. Controls on Trace Element distribution in Oxides and Silicates. *J. Petrol.* 59, 233–256. <https://doi.org/10.1093/ptrology/ogy027>.
- Eliche-Quesada, D., Sandalio-Pérez, J.A., Martínez-Martínez, S., Pérez-Villarejo, L., Sánchez-Soto, P.J., 2018. Investigation of use of coal fly ash in eco-friendly construction materials: fired clay bricks and silica-calcareous non fired bricks. *Ceram. Int.* 44, 4400–4412. <https://doi.org/10.1016/j.ceramint.2017.12.039>.
- Fisher, R.V., Schmincke, H.-U., 1984. Pyroclastic Fragments and deposits. In: Fisher, R. V., Schmincke, H.-U. (Eds.), *Pyroclastic Rocks*. Springer, Berlin, Heidelberg, pp. 89–124. https://doi.org/10.1007/978-3-642-74864-6_5.
- Galai, H., Pijolat, M., Nahdi, K., Trabelsi-Ayadi, M., 2007. Mechanism of growth of MgO and CaCO₃ during a dolomite partial decomposition. *Solid State Ionics* 178, 1039–1047. <https://doi.org/10.1016/j.ssi.2007.05.013>.
- Galán-Arboledas, R.J., Cotes-Palomino, M.T., Bueno, S., Martínez-García, C., 2017. Evaluation of spent diatomite incorporation in clay based materials for lightweight bricks processing. *Constr. Build. Mater.* 144, 327–337. <https://doi.org/10.1016/j.conbuildmat.2017.03.202>.
- Gencil, O., 2015. Characteristics of fired clay bricks with pumice additive. *Energ. Build.* 102, 217–224. <https://doi.org/10.1016/j.enbuild.2015.05.031>.
- Govindaraju, K., 1994. 1994 Compilation of Working Values and Sample Description for 383 Geostandards. *Geostand. Newslett.* 18, 1–158. <https://doi.org/10.1046/j.1365-2494.1998.53202081.x-i1>.
- Hamada, H.M., Abed, F., Beddu, S., Humada, A., Majdi, A., 2023. Effect of Volcanic Ash and Natural Pozzolana on mechanical properties of sustainable cement concrete: a comprehensive review. *Case Stud. Construct. Mater.* 19, e02425. <https://doi.org/10.1016/j.cscm.2023.e02425>.
- Hasan, M.R., Siddika, A., Akanda, M.P.A., Islam, M.R., 2020. Effects of waste glass addition on the physical and mechanical properties of brick. *Innov. Infrastruct. Solut.* 6, 36. <https://doi.org/10.1007/s41062-020-00401-z>.
- Hughes, J.J., 1995. *Studies on Sedimentary Provenance of the Intramontane Granada Basin, Southern Spain (Ph.D.)*. University of Glasgow.
- UNE-EN ISO 17892-12, Investigación y ensayos geotécnicos. Ensayos de laboratorio de suelos. Parte 12: Determinación del límite líquido y del límite plástico, 2019. AENOR Madrid, España.
- Jackson, M.D., Vola, G., Všiánský, D., Oleson, J.P., Scheetz, B.E., Brandon, C., Hohlfelder, R.L., 2012. Cement Microstructures and Durability in Ancient Roman Seawater Concretes. In: Válek, J., Hughes, J.J., Groot, C.J.W.P. (Eds.), *Historic Mortars*. Springer, Netherlands, Dordrecht, pp. 49–76. https://doi.org/10.1007/978-94-007-4635-0_5.
- Kilburn, C.R.J., 2015. Chapter 55 - Lava Flow Hazards and Modeling. In: Sigurdsson, H. (Ed.), *The Encyclopedia of Volcanoes, Second edition*. Academic Press, Amsterdam, pp. 957–969. <https://doi.org/10.1016/B978-0-12-385938-9.00055-9>.

- Knapek, M., Húlan, T., Minárik, P., Dobroň, P., Štubňa, I., Stráská, J., Chmelík, F., 2016. Study of microcracking in illite-based ceramics during firing. *J. Eur. Ceram. Soc.* 36, 221–226. <https://doi.org/10.1016/j.jeurceramsoc.2015.09.004>.
- Kreimeyer, R., 1987. Some notes on the firing colour of clay bricks. *Appl. Clay Sci.* 2, 175–183. [https://doi.org/10.1016/0169-1317\(87\)90007-X](https://doi.org/10.1016/0169-1317(87)90007-X).
- Laird, R.T., Worcester, M., 1956. The inhibiting of lime blowing. *Brit. Ceram. Trans. J.* 55, 545–563.
- Lechner, P., Tupper, A., Guffanti, M., Loughlin, S., Casadevall, T., 2018. Volcanic Ash and Aviation—The challenges of Real-Time, Global Communication of a Natural Hazard. In: Fearnley, C.J., Bird, D.K., Haynes, K., McGuire, W.J., Jolly, G. (Eds.), *Observing the Volcano World: Volcano Crisis Communication*. Springer International Publishing, Cham, pp. 51–64. https://doi.org/10.1007/11157_2016_49.
- Lecomte, G.L., Bonnet, J.P., Blanchart, P., 2007. A study of the influence of muscovite on the thermal transformations of kaolinite from room temperature up to 1,100 °C. *J. Mater. Sci.* 42, 8745–8752. <https://doi.org/10.1007/s10853-006-0192-7>.
- Lemougna, P.N., Wang, K., Tang, Q., Nzeukou, A.N., Billong, N., Melo, U.C., Cui, X., 2018. Review on the use of volcanic ashes for engineering applications. *Resour. Conserv. Recycl.* 137, 177–190. <https://doi.org/10.1016/j.resconrec.2018.05.031>.
- León, R., Palomino, D., Vázquez, J.-T., Medialdea, T., Somoza, L., 2019. A new scenario for the mass transport deposits west Canary volcanic province. *Earth Planet. Sci. Lett.* 509, 27–37. <https://doi.org/10.1016/j.epsl.2018.12.020>.
- López Gómez, M., Cultrone, G., 2023. The use of Expanded Polystyrene and Olive Stones in the Manufacture of Lightweight Bricks: Evaluation of their Properties and Durability. *Materials* 16, 1330. <https://doi.org/10.3390/ma16041330>.
- Mackwell, S.J., 1992. Oxidation kinetics of fayalite (Fe₂SiO₄). *Phys. Chem. Miner.* 19, 220–228. <https://doi.org/10.1007/BF00202311>.
- Maniatis, Y., Simopoulos, A., Kostikas, A., 1981. Moessbauer Study of the effect of Calcium Content on Iron Oxide Transformations in Fired Clays. *J. Am. Ceram. Soc.* 64, 263–269. <https://doi.org/10.1111/j.1151-2916.1981.tb09599.x>.
- Martin García, J.M., Delgado, G., Sanchez Maranon, M., Parraga, J.F., Delgado, R., 1997. Nature of dioctahedral micas in Spanish red soils. *Clay Miner.* 32, 107–121.
- Martín-Rodríguez, P., Fernández-Jiménez, A., Alonso, M. Del M., Palomo, A., García-Lodeiro, I., 2024. Valorisation of “La Palma” volcanic ash for making Portland-blended, alkaline and hybrid Portland-alkaline cements. *Materials* 17, 242. <https://doi.org/10.3390/ma17010242>.
- Mihai, R.A., Espinoza-Caiza, I.A., Melo-Heras, E.J., Cubi-Insuaste, N.S., Pinto-Valdiviezo, E.A., Catana, R.D., 2023. Does the Mineral Composition of Volcanic Ashes have a Beneficial or Detrimental Impact on the Soils and Cultivated Crops of Ecuador? *Toxics* 11, 846. <https://doi.org/10.3390/toxics11100846>.
- Modena, C., Lourenço, P.B., Roca, P., 2018. Ancient binding materials, mortars and concrete technology: history and durability aspects. In: *Structural Analysis of Historical Constructions - 2 Volume Set: Possibilities of Numerical and Experimental Techniques - Proceedings of the IVth Int. Seminar on Structural Analysis of Historical Constructions*, 10–13 November 2004. CRC Press, Padova, Italy.
- Moore, D.M., Reynolds Jr., R.C., 1997. *X-Ray Diffraction and the Identification and Analysis of Clay Minerals*, Second Edition. ed. Oxford University Press, New York, USA.
- Moseley, D., 1984. Symplectic exsolution in olivine. *Am. Mineral.* 69, 139–153.
- Muñoz, P., Letelier, V., Zamora, D., Morales, M.P., 2020. Feasibility of using paper pulp residues into fired clay bricks. *J. Clean. Prod.* 262, 121464. <https://doi.org/10.1016/j.jclepro.2020.121464>.
- Murmu, A.L., Patel, A., 2018. Towards sustainable bricks production: an overview. *Constr. Build. Mater.* 165, 112–125. <https://doi.org/10.1016/j.conbuildmat.2018.01.038>.
- Pankhurst, M.J., Scarrow, J.H., Barbee, O.A., Hickey, J., Coldwell, B.C., Rollinson, G.K., Rodríguez-Losada, J.A., Lorenzo, A.M., Rodríguez, F., Hernández, W., Fernández, D. C., Hernández, P.A., Pérez, N.M., 2022. Rapid response petrology for the opening eruptive phase of the 2021 Cumbre Vieja eruption, La Palma, Canary Islands. *Volcanica* 5, 1–10. <https://doi.org/10.30909/vol.05.01.0110>.
- Randive, K.R., Korakoppa, M.M., Muley, S.V., Varade, A.M., Khandare, H.W., Lanjewar, S.G., Tiwari, R.R., Aradhi, K.K., 2015. Paragenesis of Cr-rich muscovite and chlorite in green-mica quartzites of Saigaon–Palasgaon area, Western Bastar Craton, India. *J. Earth Syst. Sci.* 124, 213–225. <https://doi.org/10.1007/s12040-014-0514-0>.
- Shepherd, K., Namur, O., Toplis, M.J., Devidal, J.-L., Charlier, B., 2022. Trace element partitioning between clinopyroxene, magnetite, ilmenite and ferrobaltic to dacitic magmas: an experimental study on the role of oxygen fugacity and melt composition. *Contrib. Mineral. Petrol.* 177, 90. <https://doi.org/10.1007/s00410-022-01957-y>.
- Soil Conservation Service (USDA), 1972. *Methods and Procedures for Collecting Soil Samples*. Washington (US).
- Stewart, C., Johnston, D.M., Leonard, G.S., Horwell, C.J., Thordarson, T., Cronin, S.J., 2006. Contamination of water supplies by volcanic ashfall: a literature review and simple impact modelling. *J. Volcanol. Geotherm. Res.* 158, 296–306. <https://doi.org/10.1016/j.jvolgeores.2006.07.002>.
- Tan, W., Liu, P., He, H., Wang, C., Liang, X., 2016. Mineralogy and Origin of Exsolution in Ti-Rich Magnetite from Different Magmatic Fe-Ti Oxide-Bearing Intrusions. *The Can. Mineral* 54, 539–553. <https://doi.org/10.3749/canmin.1400069>.
- Tourrette, T.Z.L., Burnett, D.S., Bacon, C.R., 1991. Uranium and minor-element partitioning in Fe-Ti oxides and zircon from partially melted granodiorite, Crater Lake, Oregon. *Geochim. Cosmochim. Ac.* 55, 457–469. [https://doi.org/10.1016/0016-7037\(91\)90004-0](https://doi.org/10.1016/0016-7037(91)90004-0).
- Troll, V.R., Carracedo, J.C., 2016. Chapter 1- the Canary Islands: An introduction. In: *The Geology of the Canary Islands*. Elsevier.
- U. S. Geological Survey, 2023. Mineral commodity summaries 2023 (No. 2023), Mineral Commodity Summaries. U.S. Geological Survey. <https://doi.org/10.3133/mcs2023>.
- Verde, M., De Bonis, A., D’Uva, F., Guarino, V., Izzo, F., Rispoli, C., Borriello, G., Giglio, M., Iavarone, S., Morra, V., 2022. Mineropetrographic investigation on Roman pottery found in a dump in the workshop area of Cumae (southern Italy). *J. Archaeol. Sci. Rep.* 42, 103376. <https://doi.org/10.1016/j.jasrep.2022.103376>.
- Warr, L.N., 2021. IMA–CNMNC approved mineral symbols. *Mineral. Mag.* 85, 291–320. <https://doi.org/10.1180/mgm.2021.43>.
- White, W.M., 2020. Chapter 7: Trace Elements in Igneous Processes. In: *Geochemistry*. Wiley Blackwell, pp. 309–364.
- Wilson, T.M., Jenkins, S., Stewart, C., 2015. Chapter 3 - Impacts from Volcanic Ash fall. In: Shroder, J.F., Papale, P. (Eds.), *Volcanic Hazards, Risks and Disasters, Hazards and Disasters Series*. Elsevier, Boston, pp. 47–86. <https://doi.org/10.1016/B978-0-12-396453-3.00003-4>.
- Winkler, V.H., 1954. Bedeutung der Korngrößenverteilung und des Mineralbestandes von Tonen für die Herstellung grobkeramischer Erzeugnisse. *Berichte Deutschen Keramischen Gesellschaft* 31, 337–343.
- Zhang, L., 2013. Production of bricks from waste materials – a review. *Constr. Build. Mater.* 47, 643–655. <https://doi.org/10.1016/j.conbuildmat.2013.05.043>.
- Zheng, Q., Zhang, Y., Liu, T., Huang, J., Xue, N., Shi, Q., 2017. Optimal Location of Vanadium in Muscovite and its Geometrical and Electronic Properties by DFT Calculation. *Minerals* 7, 32. <https://doi.org/10.3390/min7030032>.